Titre: Title:	Bias-Enhanced Tungsten Oxide Films for Durable Electrochromic Devices
Auteur: Author:	Francis Blanchard
Date:	2018
Type:	Mémoire ou thèse / Dissertation or Thesis
Référence: Citation:	Blanchard, F. (2018). Bias-Enhanced Tungsten Oxide Films for Durable Electrochromic Devices [Mémoire de maîtrise, École Polytechnique de Montréal]. PolyPublie. https://publications.polymtl.ca/3115/

Document en libre accès dans PolyPublie
Open Access document in PolyPublie

URL de PolyPublie: PolyPublie URL:	https://publications.polymtl.ca/3115/
Directeurs de recherche: Advisors:	Ludvik Martinu, & Jolanta-Ewa Sapieha
Programme: Program:	Génie physique

UNIVERSITÉ DE MONTRÉAL

BIAS-ENHANCED TUNGSTEN OXIDE FILMS FOR DURABLE ELECTROCHROMIC
DEVICES

FRANCIS BLANCHARD

DÉPARTEMENT DE GÉNIE PHYSIQUE

ÉCOLE POLYTECHNIQUE DE MONTRÉAL

MÉMOIRE PRÉSENTÉ EN VUE DE L'OBTENTION

DU DIPLÔME DE MAÎTRISE ÈS SCIENCES APPLIQUÉES

(GÉNIE PHYSIQUE)

MAI 2018

UNIVERSITÉ DE MONTRÉAL

ÉCOLE POLYTECHNIQUE DE MONTRÉAL

Ce mémoire intitulé :

BIAS-ENHANCED TUNGSTEN OXIDE FILMS FOR DURABLE ELECTROCHROMIC
DEVICES

présenté par : BLANCHARD Francis

en vue de l'obtention du diplôme de : Maîtrise ès sciences appliquées

a été dûment accepté par le jury d'examen constitué de :

M. MOUTANABBIR Oussama, Ph. D., président

M. MARTINU Ludvik, Ph. D., membre et directeur de recherche

Mme KLEMBERG-SAPIEHA Jolanta-Ewa, Doctorat., membre et codirectrice de recherche

M. SCHIETTEKATTE François, Ph. D., membre externe

ACKNOWLEDGEMENTS

RÉSUMÉ

La technologie des couches minces fait partie intégrante de la vie courante mais reste tout de même largement méconnue du publique. Elle consiste à déposer des couches très minces de matériaux, de l'ordre du micron ou même du nanomètre sur un objet afin de modifier les propriétés et par le fait même, la façon dont il interagit avec le monde. Ces revêtements fonctionnels sont utilisés pour augmenter la durée de vie des outils et engins mécaniques, pour donner de la couleur et brillance à une surface, pour prévenir les égratignures et les reflets sur les lunettes, ainsi qu'une multitude d'autres applications. Un autre usage très important est pour les fenêtres écoénergétiques, où des revêtements spécialement conçus peuvent aider au contrôle de la température en modifiant leur efficacité thermique. Parmi les nanotechnologies dites "vertes" pour la fenestration existe la fenêtre intelligente, basée sur des matériaux électrochromiques ayant la capacité de moduler leur coloration par l'insertion d'ions lorsqu'un courant électrique est appliqué. En cyclant entre un état coloré et un état transparent, l'absorption thermique de la fenêtre peut être ajustée de manière à réduire la consommation énergétique pour le chauffage et la climatisation.

Ce projet s'intéresse principalement au plus connu des matériaux électrochromiques pour ses capacités supérieures: le WO_3. Puisque le WO_3 et les dispositifs électrochromiques en général ont tendance à souffrir de dégradation lors de longues périodes d'utilisation, l'objectif de ce projet est d'améliorer la durabilité du matériau en modifiant sa microstructure. Pour ce faire, nous avons préparé ce matériau par pulvérisation magnétron RF avec l'assistance d'un bombardement ionique à haute énergie généré par un potentiel électrique appliqué sur le porte-substrat.

Des échantillons ont été préparés avec et sans bombardement ionique, à haute et basse pression, puis ont été analysés par ellipsométrie, spectrophotométrie, microscopie à force atomique, microscopie électronique à balayage, microscopie électronique en transmission et voltammétrie cyclique. Ceci nous a permis d'établir qu'à des énergies assez élevées, le bombardement ionique cause des modifications structurelles importantes, particulièrement de la nanocristallisation et une porosité microstructurale. Pour des échantillons préparés à basse pression, ces changements sont jugés responsables d'une large augmentation de la durabilité par rapport aux échantillons à haute pression, tout en maintenant une structure poreuse favorable pour l'insertion d'ions et la coloration. Des travaux ont aussi été réalisés pour développer de petits dispositifs électrochromiques pour des applications d'authentification de documents importants. Des travaux futurs envisagés en lien avec

ce projet incluent une recherche approfondie sur le mécanisme de croissance du WO_3 et d'autres matériaux soumis à un bombardement ionique à haute intensité, ainsi que l'intégration du WO_3 modifié par bombardement ionique dans des dispositifs de sécurité.

ABSTRACT

Thin film technology is a critical component of many objects in our daily lives, yet remains mostly unknown to the public at large. It consists in the deposition of very thin layers of material on substrates at the micron or even at the nanometer scale to modify their properties and consequently, the way they interact with the world. These so-called functional coatings can be used to vastly augment the lifetime of tools and mechanical parts, to give color and sheen to a surface, to prevent scratches and glare on glasses as well as multitude other uses. One very important application is for eco-energetic windows, where specially designed coatings can help with temperature control by improving their thermal efficiency. Amongst these "green" nanotechnologies for fenestration is the smart window, based on electrochromic materials which possess the ability of transmission modulation following the application of an electrical current resulting in ion insertion. By switching between a colored and a bleached state, the thermal absorption of the window can be adjusted to reduce the energy required to heat or cool a building.

This work focuses mostly on the most famous electrochromic material for its superior properties: WO_3. Since WO_3 and electrochromic devices in general tend to suffer from degradation issues over repeated coloration/bleaching cycles, the aim was to improve the durability of the material by changing its microstructure. To do so, we prepared the material with RF magnetron sputtering and the assistance of a high energy ion bombardment generated by substrate biasing.

Samples were prepared at high and low pressures with and without ion bombardment and subsequently analyzed by ellipsometry, spectrophotometry, atomic force microscopy, scanning electron microscopy, transmission electron microscopy and cyclic voltammetry. This allowed us to establish that at high enough energies, the ion bombardment results in significant structural changes, most notably nanocrystallization and microstructural porosity. For samples prepared at low pressures, these changes are thought to be responsible for a large increase in durability over samples deposited at higher pressures whilst maintaining a porous microstructure favorable for ion insertion and coloration. Work was also done towards developing smaller electrochromic devices aimed towards the anticounterfeiting market. Future work based on this project includes further research into the growth mechanisms of WO_3 and other materials under high energy ion bombardment as well as integration of the biased WO_3 layers into security devices.

TABLE OF CONTENTS

LIST OF TABLES

LIST OF FIGURES

LIST OF SYMBOLS AND ABBREVIATIONS

Abbreviations

ATF	All-thin-film
AFM	Atomic force microscopy
CE	Coloration efficiency
CV	Cyclic voltammetry
CVD	Chemical vapor deposition
DC	Direct current
E-beam	Electron beam
EC	Electrochromic
ECD	Electrochromic device
ED	Electron diffraction
EDS	Electron diffraction spectroscopy
EDX	Energy dispersive x-ray spectroscopy
EMA	Effective medium approximation
ERD	Elastic recoil detection
FCSEL	Functional Coatings and Surface Engineering Laboratory
FIB	Focused ion beam
GLAD	Glancing angle deposition
HiPIMS	High power impulse magnetron sputtering
HRTEM	High resolution transmission electron microscopy
HWCVD	Hot-wire chemical vapor deposition
IR	Infrared
ISAD	Integrated surface area difference

ITO   Indium tin oxide

MIC-CSE   Multisectorial Industrial Research Chair in Coatings and Surface Engineering

MHz   Megahertz

MSE   Mean squared error

NiO   Nickel oxide

NIR   Near infrared

PVD   Physical vapor deposition

RBS   Rutherford back-scattering spectroscopy

RF   Radio-frequency

RMS   Root mean square

SAED   Selected area diffraction

SCE   Saturated calomel electrode

SEM   Scanning electron microscopy

TCO   Transparent conductive oxide

TEM   Transmission electron microscopy

UMA   Universal measurement accessory

UV   Ultraviolet

VASE   Variable angle spectroscopic ellipsometry

XRD   X-ray diffraction

Symbols

a-   Amorphous

A   Absorbance

c-   Crystalline

D_e	Electron diffusion coefficient
D^+	Cation diffusion coefficient
e	Elementary charge
eV	Electronvolt
E	Energy
E_g	Bandgap
F	Faraday constant
k	Absorption coefficient
M	Mol
n	Refractive index
n_{eff}	Medium's effective refractive index
N_A	Avogadro's number
q_{ext}	Extracted charge
q_{ins}	Inserted charge
N	Perfect gas constant
R	Reflectance
ΔT	Transmittance modulation
T	Transmittance
ε	Permittivity constant
λ	Wavelength
v	Frequency

LIST OF APPENDICES

CHAPTER 1   INTRODUCTION

1.1   Energy consumption and control – smart windows

The world is driven by its energy consumption; advanced economies are especially energy-based, and the future will depend on our ability to meet the energetic demand. In 2016, the world's total energy consumption reached an estimated 13 276.3 million tons of oil equivalent, or about 94.8 billion barrels of oil. While this number has grown at a reduced rate in recent years [1], we are still burning non-renewable resources at an alarming rate.

Thus, we are witnessing a considerable growth in interest, both in academia and in industry, to improve and promote the use of alternative and greener technologies such as wind power, solar cells and hydro-electricity amongst others [2]. While this is a necessary step to ensure that we do not remain fully dependent on finite and environmentally damaging resources, the way forward does not simply lie in changing how we produce energy. If we are to meet growing demands due to the ever-growing population, we must also look at how this energy is spent. In addition, as technology advances, people are getting accustomed to a higher standard of living, which is almost always accompanied by a corresponding increase in how much energy is needed to sustain it.

This is especially true for the living accommodations we create. Therefore, it is no surprise that a 2007 study by the United Nations attributed between 30-40% of energy expenditure to the building sector [3], whether commercial or residential. This consists mostly of our efforts to control living conditions related to heating, cooling, lighting, ventilation and more. After all, people nowadays spend most of their time indoors, in North America at least [4]. This task is especially arduous in regions where climates are extreme or show significant variations throughout the year, as well as for buildings without sufficiently high energy efficiency standards. A significant way to reduce the world's energy consumption and contribute to improving its energetic situation is, therefore, to reduce the burden imposed by our living environment.

Recent architectural tendencies have increasingly promoted the use of window facades, particularly for high-rise towers easily found in any city around the globe. Living spaces in general also feature more windows as people desire some form of natural lighting and visual contact with the outside world. They have also been shown to reduce psychological discomfort in the workplace [5] and are more attractive for commercial facades to display products and attract customers. But all of

these advantages do come with a drawback; namely, windows are usually the weak link in a building's isolation [6]. This means, that as more and more windows are added to a structure's exterior walls, temperature control costs also increase. It then becomes clear that more thermally efficient windows are a priority to control and reduce energy waste. There are, consequently, significant advantages, both environmentally and economically, to developing and improving highly insulating windows.

The main way this has been achieved over the years is by adding optical thin films (glazings) to architectural glass to filter and control the energy transfer. When designing a window for energy control, it is imperative to consider the most important glazing factors: transmittance (UV, visible and solar), reflectance and emissivity, which together give the solar heat gain coefficient, a measure of the total heat capable of passing through the window [7]. Figure 1.1 shows the solar spectrum and its black body radiation curve at 5762 K, detailing which wavelengths are most present in the light we seek to control. Since we want to keep visible light transparency as high as possible, it is the NIR part that must be controlled.
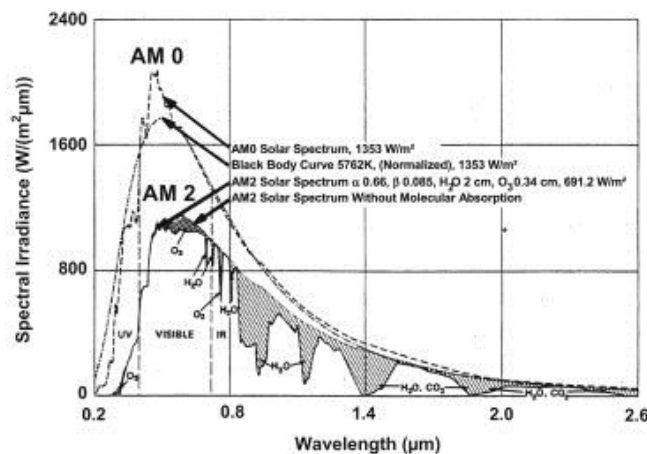
Figure1.1.1: The radiation from the sun, comparing the AM0 (outer space) and AM2 (at the earth's surface, the sun above the horizon) spectra. The AM2 spectrum is shown both with and without molecular absorption (in O_2, O_3, H_2O and CO_2). Redrawn from Fahrenbruch and Bube. Taken from [7].

A well known example of solar filters are the low-emissivity coatings, which are usually based on thin silver or transparent conductive oxide films [8]. They are specifically engineered to be very

reflective at infrared wavelengths, preventing heat from passing through and escaping during cold days or entering during hotter periods.

One way to improve the temperature control of optical coatings is to move from passive to active technologies. Instead of relying on the passive properties of materials to reflect a certain percentage of light, we can instead build thin film devices that are adjustable. By applying external stimuli, which can be pressure, light, heat, electrical potential or gas, some materials exhibit a change in their optical properties. These materials are defined as chromogenic for their ability to produce a visible or NIR transmittance change when the proper conditions are met. Upon removing the stimulus, or applying it in reverse in the case of a voltage, the device goes back to its original state. Integrating this type of material into the design of a window's coating results in so-called "smart"
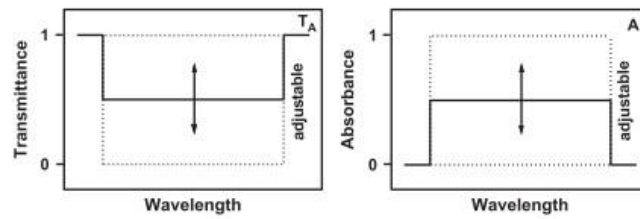
Transmittance modulation (T_A) by regulation of the absorbance (A).
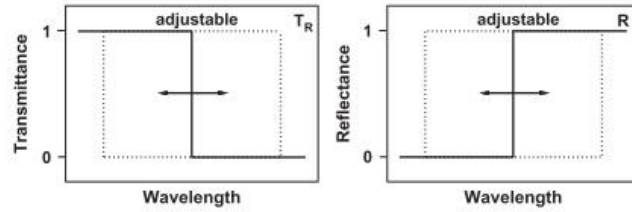
Transmittance modulation (T_R) by regulation of the reflectance (R).
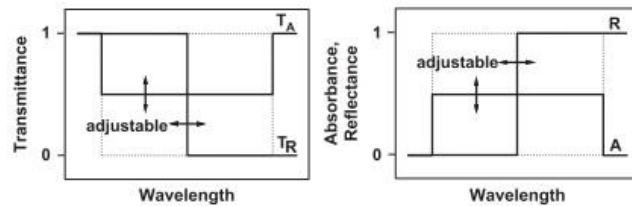
Transmittance modulation (T_A and T_R) by combined regulation of both the absorbance (A) and the reflectance (R).

Figure 1.2: Transmittance modulation by regulation of absorbance (*A*), reflectance (*R*) and both. Adapted from [7].

windows, which can be used to modulate the transmittance at desired wavelengths through changes in absorbance, reflectance or both (see Figure 1.2).

One of the most studied materials for this type of application is tungsten trioxide (WO_3) [6], [9], an electrochromic material which upon the application of an electrical potential changes from a transparent to dark blue state due to an increase in absorption in the red and near-infrared parts of the spectrum (see Figure 1.3. for an example of a window in different coloration states).

Figure 1.3: Coloration sequence of an electrochromic window [57].

A controlled amount of light is allowed to pass through depending on how dark the device is, and the level of coloration is controlled by the intensity and length of the applied voltage pulse. This allows for a precise control over the solar heat gain of the window. Moreover, since the modulation also affects the visible part of the spectrum, one can envision the use of this same technology for privacy, light intensity control and user comfort. Compared to other types of chromogenic materials, WO_3 also has the advantage of being user controllable and of being unaffected by light or temperature variations present in most real-life environments. It is also possible to power the device by simple means, requiring only a few volts of potential and minimal current to function, meaning that it can be implemented in most situations and might even be powered by another integrated device, such as a solar cell [10]. The device will then maintain its properties unless the reverse potential is applied, in a battery-like memory effect. More will be explained on the functionality of such devices in section 2.2.

The goal is to one day get to the point where a brick wall and a window façade posses similar thermal efficiencies. Presently, however, electrochromic devices have a few weaknesses over their passive counterparts: mainly high production costs and durability issues. On top of that, windows are, by design, meant to be installed and then forgotten but they are still held to incredibly high

standards and expected to last for decades. While this is feasible for more traditional low-e coatings, a smart window equipped with and advanced and dynamic nanotechnology-based thin film is much more susceptible to wear and tear. When held to such high standards, present EC devices are found lacking and a need for improved durability becomes apparent [9].

1.2 Context of the research

Climate change and the dangers that come with it is a subject that is very present on the mind of people around the world, who are more and more made aware of it. As there is an obvious link between fossil fuels, the world's principal energy source, and the rapid deterioration of our ecosystems, it seemed to me that tackling the very wasteful ways we produce and use power was of considerable importance.

At the same time, through my years of studies at Polytechnique Montreal, I became aware of the world of thin films and their many uses through presentations of Prof. Martinu's laboratory. Fascinated by their research, I was initially introduced to the field of EC materials through a summer internship focusing on interference-based optical security devices. A research project on the use of smart windows to improve energy efficiency seemed very interesting.

WO_3 is the most promising material and one of major interest for Guardian Industries, one of the world's top suppliers of architectural glass and a competitor of Saint-Gobain, Pilkington and Asahi Glass Co. With this industrial partner of the Multisectorial Industrial Research Chair in Coatings and Surface Engineering (MIC-CSE) chair interested in smart windows, we focused on improving some of its major flaws. Extensive research had previously been done by members of the laboratory on the best deposition conditions for the preparation of WO_3 by sputtering [11]. In addition, previous work had shown that it was possible to improve the optical performance of WO_3-based devices by transforming the single WO_3 film into a dense and porous EC interference filter[12]. However, as the coloration mechanism of WO_3 is triggered by the double insertion of electrons and ions [12], charge trapping was shown to a be problem in such multilayer architectures. We thus sought to develop a coating of WO_3 with a much higher density which would impede the flow of protons while maintaining the required electron conductivity; this would allow us to isolate the electrochromic effect in the most appropriate layers.

One of the chosen avenues was to explore the use of substrate biasing, which results in ion bombardment of the sample's surface during deposition and is known for increasing the density of the resulting film [13], [14]. As part of our methodology, we prepared films with substrate bias voltage going up to several hundred volts at low pressures as typical films are deposited at high pressures to ensure the generation of a porous microstructure. My initial results at low voltages showed the expected decrease in electrochromic activity. Only when increasing the bias voltage to much higher values did interesting effects occur.

In fact, after reaching a threshold potential, we started observing a behaviour which was opposite to the one expected for a denser layer. Instead of inhibiting the electrochromic effect, we suddenly obtained a layer that was not only highly efficient electrochromically but also much more durable than what had been observed during previous research [11], [15] (see figure 1.4).

Sensing how these results could potentially impact the field as well as intrigued by their counter intuitive behaviour, we shifted the focus of the project towards understanding what caused an improvement in performance of WO_3 layers when very high energy ion bombardment was involved.
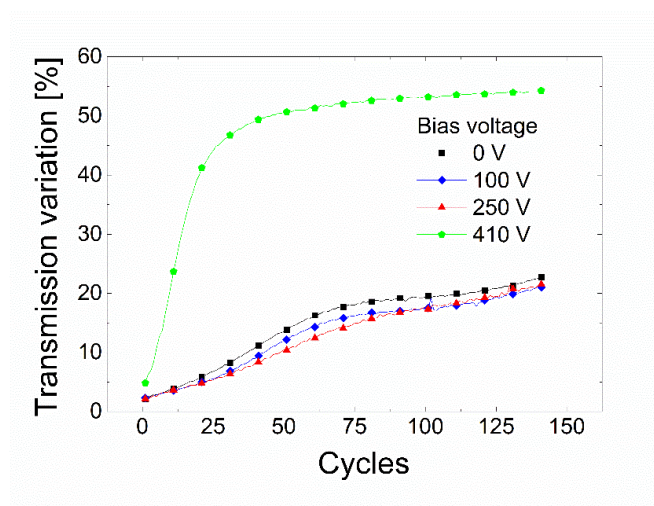
Figure 1.4 : Transmission variation (ΔT) of preliminary samples of WO_3 prepared with various applied substrate bias values.

1.3 Objectives

With the overall aim of improving the durability and performance of electrochromic WO_3 thin films, the **main objective** of my project was defined as follows:

- Investigate the effect of high energy ion bombardment on the microstructure of WO_3 thin films and their resulting electrochromic properties and durability.

To achieve this objective, a series of **specific objectives** were then defined:

1. Prepare WO_3 thin films by magnetron sputtering while varying the applied substrate bias voltage.
2. Compare the resulting films' electrochromic performance with the reference best-performing non-biased porous samples previously developed in the laboratory.
3. Analyse the composition, optical properties and microstructure of the produced samples.
4. Establish a link between the effects of ion bombardment and the resulting structural changes in the WO_3 thin films.
5. Evaluate which microstructure leads to the most efficient electrochromic behaviour coupled with the highest durability and why.

1.4 Scientific publications

Since common understanding of the use of substrate biasing would suggest a densification and deterioration of the EC performance of the films, the unexpected results we obtained formed the basis for an original research article that was submitted to the journal *Applied Materials Today* (see Table 1-1).

Table 1-1: Article accepted for publication in the context of my master's research project.

F. Blanchard, B. Baloukas, L. Martinu. *Highly durable electrochromic tungsten oxide thin films prepared by high rate bias-enhanced sputter deposition,* Applied Materials Today, 2018.

This research was also performed within the framework of the MIC-CSE chair and the results were judged as sufficiently of interest to apply for a patent to protect this discovery (see Table 1-2).

Table 1-2 : Submitted patent related to the research project

No. PCT/US2017/050621 **Title: Durable Electrochromic Device Including Tungsten Oxide Film Prepared In High Ion Bombardment And Low Pressure Deposition Environment, And/Or Methods Of Making The Same**

In addition to these publications concerning the main objective, additional work on integrating WO_3 in thin film all-solid-state devices in the context of an INNOV grant on active security devices has lead to a presentation at the Society of Vacuum Coaters' (SVC) 2017 technical conference, as well as an associated proceedings paper (see Table 1-3).

Table 1-3 : SVC proceeding paper

F. Blanchard, B. Baloukas, L. Martinu , *All-Thin-Film Multi-Color Electrochromic Devices,* 60th Annual Technical Conference Proceedings © 2017, Society of Vacuum Coaters Providence, Rhode Island, April 29-May 4, 2017

1.5 Thesis outline

Following the introduction, Chapter 2 of this thesis will present a literature review as well as the theoretical background required to understand the body of the work. Electrochromism plays a major role, with sections dedicated to its history, the functioning of an electrochromic device, the different materials that exhibit this behaviour, the effect of porosity on their performance, and the differences between amorphous and crystalline materials. A second part will focus on the fabrication methods of electrochromic thin films, such as e-beam evaporation and sol-gel, with a focus on sputtering. This will be mostly aimed towards how we can achieve a specific microstructure by controlling the deposition conditions.

Chapter 3 consists of the experimental methodology that was used throughout this project. To begin with, the bias-assisted RF magnetron sputtering process will be described, followed by the different

methods of optical characterization that were used. Afterwards, electrochemical and physical characterization methods will be presented.

Chapter 4 is dedicated to the article that was submitted for publication regarding the main objective of this research, which is presented as it was sent to the journal.

Chapter 5 will further discuss the results presented in the article and offer some additional perspectives. Nanostructured crystalline WO_3, some other possibilities for high energy substrate biasing as well as a brief overview of my work on active security devices are the themes touched upon.

Finally, Chapter 6 offers conclusion and recommendations for future research avenues.

CHAPTER 2   LITERATURE REVIEW AND THEORETICAL BACKGROUND

2.1 Foreword

This chapter presents the main theory and knowledge background in relation to the principal findings of this research. Electrochromism is a relatively well-known but not yet fully explored phenomenon that continues to attract the attention of a number of many researchers' efforts around the world. Therefore, a significant amount of information may be found in the literature, either in journal articles or in books. While the most pertinent elements will be covered in this section, the reader interested in learning more on the subject is encouraged to consult the *Handbook of Inorganic Electrochromic Materials* by C.G. Granqvist [16] and *Electrochromism and Electrochromic Devices* by P.M.S. Monk, R. Mortimer and D. Rosseinsky [17] as excellent resources.

The present chapter focuses on thin film inorganic electrochromic materials. A brief history of electrochromic (EC) materials first introduces the context in this research takes place. An explanation of the phenomenon and how such films may be incorporated into functional devices follows.

WO_3, as a model EC material, is then studied more in depth. Information on its atomic structure is given, as well as an explanation of the importance of controlling the microstructure of such films to achieve appropriate device performance. Finally, a comparison between the amorphous and crystalline phases of WO_3 highlights their respective advantages and disadvantages.

Since the core of my project was directed towards modifying traditional deposition approaches by the addition of substrate biasing, a second section concerning the most popular fabrication methods of WO_3 films follows. While e-beam and sol-gel preparation methods are briefly described, most of the information relates to sputtering and how a thin film's microstructure and resulting properties can be controlled through a judicious control of the deposition conditions. Special emphasis is then put on the impact of ion bombardment as this clearly relates to our findings.

2.2   Electrochromism

The term electrochromism refers to, as the name suggests, coloration and electricity. More specifically, it describes the coloration phenomenon that some materials undergo when an electric potential is applied to them. As will soon be demonstrated, the coloration mechanism is related to an increase (reduction) or decrease (oxidation) in the number of electrons in the atomic system of such materials. Indeed, the displacement of these excess charges between energy levels following excitation is what causes the change in optical properties [16].

While there exist two main types of electrochromic materials, either organic or inorganic, only the latter ones are of interest in the present context due to several reasons. Indeed, although organic materials can exhibit faster coloration dynamics and more varied color changes, they suffer more from degradation than their inorganic counterparts [18]. Since device lifetime is of primary concern for smart windows, and considering this laboratory's main expertise on inorganic thin films, the choice was clear. Of all the inorganic materials, the most famous of them is WO_3, due to it being one of the first materials to be studied for this behaviour and its high coloration efficiency.

2.2.1   Historical background

The discovery of EC materials dates back to around 1704, when a painter named Diesbach discovered Prussian blue, a type of ferrocyanide that was largely used as a pigment in paints and inks [17]. Later on, the first demonstration of WO_3 color changing properties was made by Berzelius in 1815, where the material heated in a hydrogen atmosphere switched from pale yellow to dark blue [19]. It was not until 1930 that the first electro-reduction of solid-state WO_3 in an acid electrolyte, the same method that is used today to characterize the material, was realized by Kobosew and Nekrasson [17].

The first electrochromic device (ECD) is widely recognized as the prototype proposed by S.K. Deb in 1969 [17], [19]. Consisting of an amorphous WO_3 thin layer evaporated on a quartz substrate, the color change was observed in plane upon applying an electrical potential between two regions. The particularity of this type of device was that there was no ion reservoir in contact with the layer, neither solid nor liquid. It was rather the ambient humidity that served as a hydrogen source, where moisture adsorbed on the surface of the device was dissociated upon the application of the electric current. This work by Deb then served as the basis for a multitude of applications involving

tungsten oxide. Early on, display systems were considered but none ever made it to commercialization mainly due to durability and switching speed issues. The first real commercial success was rear-view mirror with variable reflectance for the automotive industry [16], while present day efforts are mostly aimed towards smart windows.

2.2.2 Electrochromic materials

There exist three different types of electrochromic materials. There are materials that are soluble during their utilization, while others are soluble in their transparent form and solidify on the electrode after the coloring reaction. For practical reasons, when trying to build thin film-based devices both of these are not suitable. The third type of material which always remain solid is therefore favored – they include a range of transition metal oxides. Figure 2.1 displays which of these materials have a cathodic, anodic or dual behavior as in the special case of vanadium oxide [16].
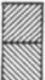
Figure 2.1: Simplified periodic table of elements. Grayed transition metals are those with well documented cathodic and anodic electrochromism. Taken from [16].

While many different elements are capable of EC reactions, each has its own properties. The two most popular EC oxides are by far cathodic WO_3 and anodic NiO, for the simple reason that they possess the highest coloration efficiency of their respective categories. WO_3 is a cathodic EC material which is transparent in its natural state and displays a deep blue color upon ion intercalation. Nickel oxide is an anodic EC material which displays a yellow-brownish color in its colored state and becomes transparent upon ion intercalation.

Not much work was put into studying NiO during this master's project as I focused my attention on WO$_3$. However, NiO films were developed and tested in the context of all solid-state devices implemented for security applications as will shortly be discussed in Chapter 5.

2.2.3 Coloration mechanism

Let us now consider the mechanism behind the materials' coloration. Upon the application of a voltage, electrons are inserted into the material and due to their negative charge, positively charged ions are then attracted maintain neutrality. It is this double charge insertion that leads to coloration in inorganic materials [20]. For cathodic EC materials, a simplified version of the reaction may be written as follows in the context of WO$_3$:

$$WO_3 + x\,(M^+ + e^-) \leftrightarrow M_x WO_3 \tag{1}$$
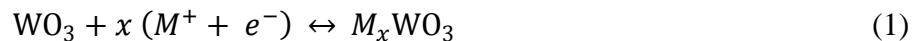
where M_+ is a cation, x is the intercalation level and $M_x WO_3$ is the colored bronze state of WO$_3$.

This process is called ion intercalation and usually involves small cations such as H$^+$ or alkalines, such as Li$^+$ and Na$^+$ which diffuse into the material [21], [22]. A similar but reversed reaction is observed for anodic materials, which switch to a transparent state upon ion intercalation. For NiO, the hydrogen ion intercalation/deintercalation reaction can be summarized as follows:

$$Ni(OH)_2 - xH^+ - xe^- \leftrightarrow NiO_x(OH)_{2-x} \tag{2}$$
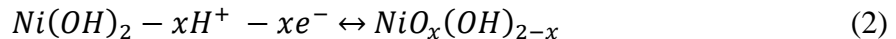
where NiOOH is strongly absorbing and the form Ni(OH)$_2$ with an added cations is transparent [16].

From equation 1, we can already conclude that EC materials must be able to conduct electrons and allow for ionic diffusion. The physical reason why this charge insertion results in a color change, and why anodic and cathodic materials behave differently lies in their electronic configuration. Taking bleached WO$_3$ as an example, when no charges are intercalated, the material is transparent in its semi-conductor state; this transparent state is typical of any semi-conductor with a large enough bandgap. For WO$_3$, the bandgap lies in the UV at ~3.2 eV [23] while the Fermi level is under the conduction band between oxygen's *2p* and tungsten's *t$_{2g}$* orbitals [22] (see Figure 2.2 which presents the band diagrams of cathodic and anodic electrochromic materials) The t$_2$g orbitals

correspond to the d_{xy}, d_{xz} and d_{yz} orbitals of a transition metal whose *s* and *p* electrons are fully ionized.
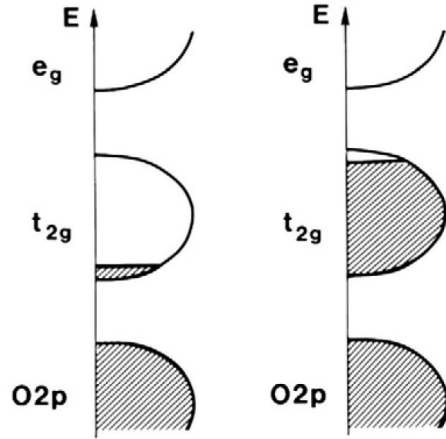
Figure 2.2: Schematic band structure of different categories of EC oxides, cathodic (left) and anodic(right). Shaded regions denote filled states and E denotes energy. Taken from [16].

When ions and electrons are injected in a cathodic material, the t_{2g} orbitals are the first to be filled as they are more energetically favorable and the Fermi level rises into the t_{2g} orbital. At this point, WO_3 becomes blue (H_xWO_3) either through an increase in absorption in the case of amorphous WO_3 (*a*-WO_3) or an increase in reflection for polycrystalline WO_3 (*c*-WO_3) both in the red and near-IR parts of the spectrum. Upon extraction, the Fermi level goes back down into oxygen's *2p* orbital and the material becomes once again transparent. For anodic materials, the Fermi level is already in the t_{2g} orbital because of free electrons thus explaining their colored state. When sufficient charges are inserted, the Fermi level rises above the t_{2g} orbital and below the e_g band; providing the band gap is large enough and not in the visible, the material becomes transparent.

Even though the coloration mechanism is still not entirely understood, the most accepted models make a distinction between the two phases. For crystalline WO_3, the optical transition is caused by the electron band structure occupation change previously described, meaning that the electrons are free or quasi-free as in the Drude theoretical model. This model is also used to explain the behavior of metals, which are, in most cases, IR reflectors.

The amorphous material is instead described in terms of an intervalence charge transfer where the electrons are localized. Once a cation is intercalated, it is more favorable for it to form an OH group

than a H$_2$O molecule, until all oxygen atoms have been paired [24]. The W atoms will then switch between oxidation levels, with the charge transfer being powered by the absorption of incident photons, with the following reaction equation [25], [26]:

$$W_i^{6+} + W_j^{5+} + hv \leftrightarrow W_i^{5+} + W_j^{6+} \tag{3}$$
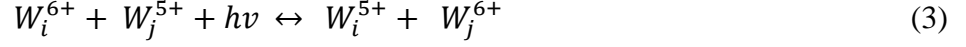
Reduction to a W^{4+} state is also possible but requires two electrons to reach the same site and is less probable. Transitions between these three states also mean different absorption mechanisms and the transition to that twice reduced state has also been identified as the main source of coloration in nanocrystalline WO$_3$ synthesized via a sol–gel based dip coating process [25].

2.2.4 Electrochromic devices

Now that we know that double charge insertion is responsible for coloration, we must find a way to design a thin film stack that allows such a process to take place. Typical devices have two electrodes, an electrochromic layer, an electrolyte layer and an ion storage film. To be able to observe the color change, at least one of the electrodes needs to be transparent, which can be achieved with transparent conductive oxides (TCOs; e.g.: indium tin oxide (ITO), conductive nanowires, etc.). The substrate can be glass, in the case of a rigid device, or polymer sheets, for a
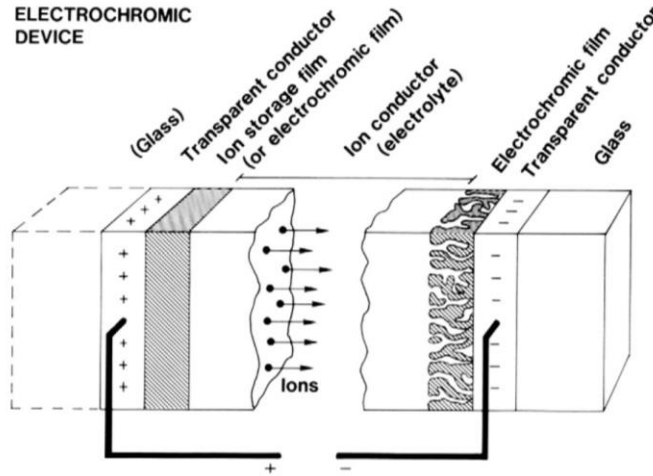
Figure 2.3: Generic five-layer electrochromic device design. Arrows indicate the movement of ions in an applied electric field. Taken from [16].

flexible version which allows roll-to-roll coating deposition. Figure 2.3 illustrates a popular configuration in the context of smart window applications.

When a negative potential is applied to the electrode in contact with the EC layer, electrons are injected into the EC layer and the cations leave the ion reservoir to complete the reaction described in Section 2.2.3. To be able to reach the active layer and counterbalance the charges, the ions must diffuse through an electrolyte layer that also serves as a barrier for electrons. This way, the charges are kept in the active layer even when the potential ceases to be applied and the device maintains its coloration (so-called memory effect). To revert to the device's initial transparent state again, or in other words bleach it, the device may be short-circuited or the potential simply inverted, thus extracting the electrons and ions from the active layer, the latter returning to the ion storage layer.

The electrolyte can be in liquid form, an acid for example may serve as a very efficient hydrogen source, in polymer form, which is extensively used in the context of flexible devices or in solid form. Polymer electrolytes decrease the probability of short-circuits because of their much larger thickness. Each form has advantages and disadvantages and must be chosen depending on the application. Electrochromic windows or glasses, for example, can pose the risk of breaking in proximity with people; using an acid as the electrolyte is then unacceptable. Some popular materials for electrolyte layers include SiO_2, Ta_2O_5 and polycarbonate polymers containing a lithium salt, e.g. $LiClO_4$ [16].

An interesting modification to this design is to implement an EC layer that is complementary to the active layer as a replacement of the ion reservoir, meaning that de device now has both anodic and cathodic EC materials. WO_3 and NiO are most often the materials that are chosen for this configuration; NiO also being the most efficient inorganic anodic EC material. As both materials will now switch at the same time, WO_3 turning blue during ion insertion and NiO turning brown upon ion extraction, the overall absorption will be higher and the resulting color will be more neutral than in the case of a single WO_3 film. When inverting the potential, both materials will once again regain their transparency as the ions flow back from WO_3 to NiO. Thus, by choosing the materials according to their tint it is possible to increase our control over the color of the whole device. Also, since hydrogen is often a critical component used to stabilize NiO into a favorable structure [16], it naturally lends itself to being a proton container for WO_3. Note that the hydrogen

can be directly inserted during the deposition process, allowing for the entire deposition of a thin film device without the need to chemically add the cations before its completion.

This type of device typically requires only a few volts to operate [16] and behaves as an open-circuit memory. Indeed, in the absence of current leaks, the desired level of coloration can be maintained without the use of additional power; in practice, current leaks are always present so that charge replenishing is required at specific intervals; still, minimizing these periods reduces the overall required power. An analogy between the EC device (ECD) and a battery is often made [26], [27] as the former also stores charges in addition to displaying an optical change. For real-life applications, these devices require a battery-like behavior to limit power consumption with the addition of minimal degradation over extended periods of time and following cycling. One example of present day smart window technology is applied to existing windows in the form of a foil, as shown in Figure 2.4 [26].
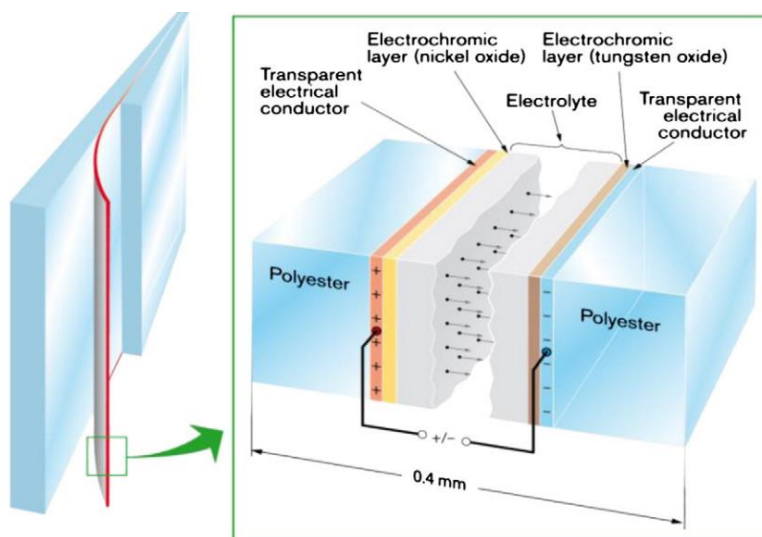
Figure 2.4: Principle of a construction of a foil-based EC device. The entire foil can be used to laminate glass panes, as shown in the left-hand part. Taken from [26].

This particular configuration uses a thicker polymer-type electrolyte and can be expected to function for thousands of cycles with a stable transmission variation between the bleached and colored states (see Figure 2.5). Industry standards typically require a 10-20 years lifetime, corresponding to hundreds of thousands of cycles with minimum degradation. This represents a significant challenge which requires constant improvement in the properties of the participating

layers, particularly regarding the active EC WO_3 layer for which durability issues are often reported [9], [12], [28].
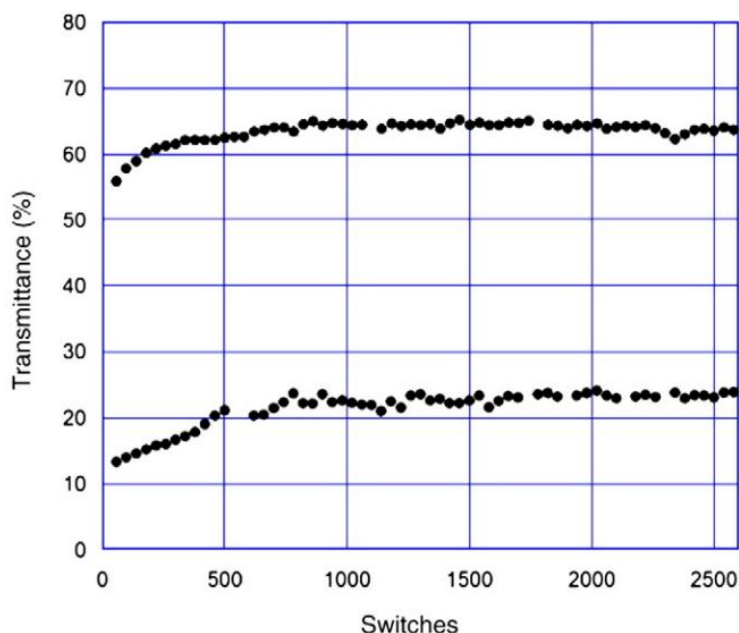
Figure 2.5: Transmittance for an EC foil device of the kind shown in Fig. 2.3 adjusted to a transmittance modulation ΔT of 55%. The panel shows evolution of the maximum and minimum transmittance during extended color/bleach cycling. Taken from [26].

2.2.5 Improving WO_3 as an electrochromic material

Now that we know what EC materials are, how ion intercalation is responsible for their color change, and how a thin film device can allow such intercalation processes, we now focus our attention on the means to improve the device's efficiency. To do so means finding ways to improve cations diffusion in and out of WO_3 to achieve faster coloration speeds, whilst maintaining or improving the lifetime.

While many factors can influence cation displacement, ion diffusion is usually the one limiting the efficiency of an ECD [15]; one should note that electron diffusion coefficients are significantly higher, as fast as to 10^{-3} cm^2/s in WO_3 [15]. To improve the former characteristic, it is necessary to look at how the atomic structure impacts the insertion and extraction dynamics. Tungsten oxide's crystalline structure is perovskite-like [29], which means it is composed of octahedral assemblies of a central tungsten atom surrounded by six oxygen atoms. These octahedra can either be joined

by their corners or by their sides and the space in between them, called a B-site, can host small ions such as H^+ or Li^+ (see Figure 2.6) [23].
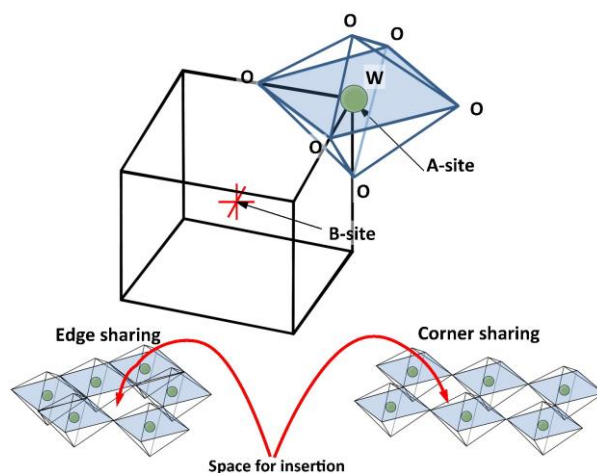
Figure 2.6: Microstructure of WO_3. Taken from [23].

2.2.5.1 Porosity and performance

Naturally, for coloration to occur the cations must be able to reach these B-sites. A more efficient coloration process implies that it is easier for the ions to reach these sites and can be achieved by the addition of defects, which will disorganize the structure and facilitate ion insertion, and/or porosity in the material. For example, increasing a layer's surface over volume ratio allows for more access points for the electrolyte to inject the ions into the WO_3, especially when using a liquid electrolyte. For this reason, control over the microstructure of the prepared thin films is of the utmost importance for electrochromic materials.

A higher porosity typically leads to a film with deeper and faster coloration, but also lower mechanical and electrochemical durability. It is therefore necessary to reach a compromise between efficiency and durability, especially in the case of applications requiring thousands of activation cycles. This is even more important in the case of devices based on H^+ insertion as such ions are known to potentially lead to damaging side reactions [15], [30]. In the context of sputtering, thin films of WO_3 are usually prepared in their amorphous phase.

Apart from changing the growth process of the layer by varying the deposition pressure, there are other ways of inducing porosity in a thin film. One of these is to introduce defects in the microstructure, which can be achieved by inserting inclusions of an atom with a bigger lattice

parameter (Mo for example) in the material [17]. Perturbing the growth in such a way results in a more disorganized layer and in more space between the WO_3 octahedra for ion diffusion. High energy ion bombardment can also cause similar defects by displacing atoms on the surface of the film as it grows. This method was extensively studied in the present project and will be discussed further in section 2.3.4.

2.2.5.2 Amorphous vs crystalline WO_3

As previously mentioned, electrochromic WO_3 is usually prepared in its amorphous phase. The main reason for this is a significant decrease in diffusion coefficient for the crystalline material. Indeed, a-WO_3 grows as clusters of edge or corner sharing octahedra [16], meaning that there is a short-range order in the microstructure and that the layout is similar to the hexagonal crystalline phase (see Figure 2.7) [31]. This results in a material where the ions can easily move around the lattice and reach the insertion sites because of the large-scale disorder.
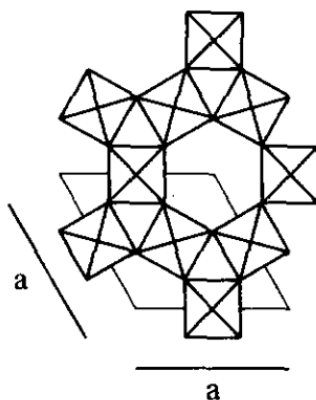
Figure 2.7: Crystal structure of hexagonal WO_3. Adapted from [31].

Conversely, WO_3 prepared at high deposition temperatures or post-annealed will crystallize in a very ordered and much denser manner, leaving very little space for the ions to travel through. The diffusion coefficients for hydrogen ions are evaluated at $\sim 10^{-8}$ cm^2/s in a-WO_3, compared to approximately 10^{-10} cm^2/s in c-WO_3 [17]. In practice, this means that a crystalline film will display little to no coloration compared to an amorphous film under the same conditions. This is even more of a problem when lithium ions are used for coloration, a very popular alternative due to reduced

degradation from side-reactions. Diffusion coefficients for Li^+ are typically in the range of 10^{-11}–10^{-10} cm^2/s for denser layers up to the range 10^{-9}–10^{-8} cm^2/s for more porous ones [24].

To be able to properly use crystalline WO_3 as an electrochromic material, it is necessary to increase its porosity. An alternative is to produce a crystallized self-assembled mesoporous structure as was done by Sallard *et al.* (see Figure 2.8)[32], but this requires an additional sol-gel or other structuring procedure which is unrealistic for large-scale production using current industry standards.

The advantage of going through the effort of producing a porous c-WO_3 is that a crystalline material is expected to be much more durable than an amorphous one and thus less subject to degradation over time. Another potential advantage in the case of smart window applications is that instead of becoming more absorbing as in the case of a-WO_3, the intercalation process mostly increases the materials reflectivity in the red and near-IR regions, granting the film with low emissivity properties.
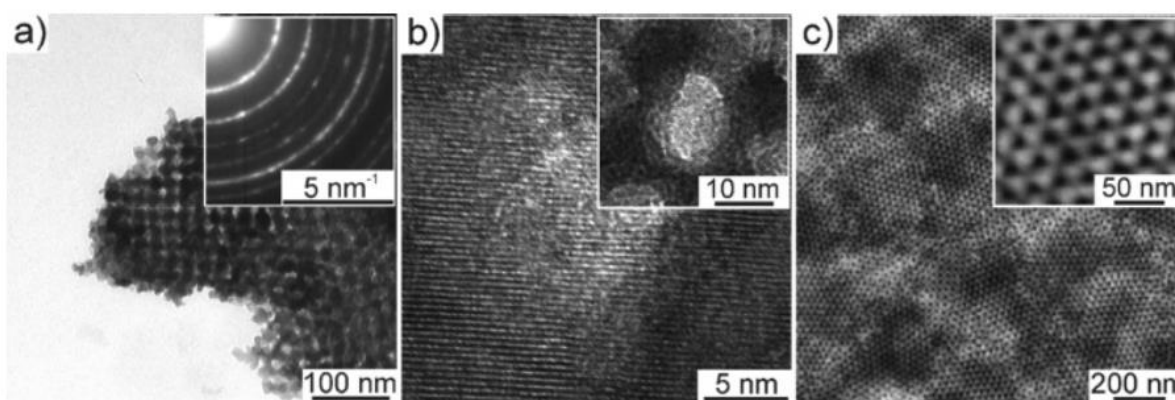
Figure 2.8: Characterization of periodically ordered WO3 thin films after crystallization at 550 °C. Part a) shows a TEM image, which demonstrates the homogeneity of the mesopore structure. The inset presents an electron diffraction (ED) pattern recorded from the same localized area. Part b) shows two HRTEM images. Both ED and HRTEM confirm the high crystallinity of the pore walls. Part c) presents tapping mode AFM images, which show hexagonally arranged open pores at the surface. Taken from [32].

In summary, regardless of the coloration mechanism, ion intercalation is required to ensure the functionality of electrochromic materials. This means that thin films must be prepared keeping in mind that sufficient porosity is needed for adequate ion mobility and therefore for coloration to be

achieved. Although amorphous materials deposited at high pressure achieve this easily enough, to improve durability, a denser and/or crystalline material is favorable. To function, however, they require induced porosity in the microstructure, possibly by creating defects. This next section is therefore dedicated to understanding more about the thin film growth processes and how one can influence film properties by controlling the deposition conditions.

2.3 Fabrication methods

Thin film deposition technology covers a very broad range of applications, from highly resistant mechanical hard coatings to finely tuned optical filters. While niche applications may require specialty coatings using a specific deposition technology, most often, researchers have the choice of various deposition techniques to develop their coatings. That being said, each technique has its own advantages and disadvantages which need to be assessed in order for the resulting thin films to comply with the application requirements.

For a number of these techniques (mostly chemical and physical vapor deposition (CVD and PVD) processes), the system must be maintained under vacuum during deposition. Otherwise, at ambient pressure the mean free path would simply be too short for the particles to be able to reach the substrate. Vacuum is also critical to avoid any chemical side reactions between the deposited species and contaminants by limiting their presence. This is especially relevant for deposition of metals, where the presence of air (mostly nitrogen and oxygen) can lead to oxidation of aluminum or nitriding of titanium during their deposition, for example.

Sputtering was chosen as our preferred means of deposition as commercial viability was important; indeed, it is the preferred large scale industrial deposition technique for our industrial partner involved with this project, Guardian Industries. In the present context, controlling the microstructure of the film is what mainly interested us so the following section covers the well-known structure zone model as well as a literature review of the impact of ion bombardment on the growth of thin films. Nevertheless, a brief overview of other popular methods of WO_3 thin film deposition is important to understand what they can offer in terms of structure control.

2.3.1 Electron-beam evaporation

As a physical vapor deposition technique, electron beam evaporation (a.k.a. e-beam evaporation) usually consists in a system where a crucible filled with the desired material is heated by an

accelerated electron beam, resulting in sublimation of the target material and subsequent precipitation of the vapor onto the substrate. By having more than one electron gun and target, co-deposition of two materials can be achieved.

One of the advantages of e-beam evaporation is that it takes place at very low pressures, meaning that no additional gases injection is required to preserve the stoichiometry of the material. This also results in a line-of-sight process, meaning that there is directionality to the growth of the film, which can be alleviated with rotation and translation of the sample holder if desired. This effect can be exploited to create interesting microstructures using the GLAD (glancing angle depositions) technique, which results in a columnar growth because of shadowing effects, with the amount of porosity depending on the relative angle between the incident material flux and substrate [12]. In addition, the voids can be filled with another material to create a composite layer.

Evaporation systems and GLAD in particular have the advantage of potentially producing more porous materials than sputtering, resulting in greater values of ion diffusion coefficient; Table 2-1 gives values for evaporation, sputtering and sol-gel (data from [16]). The material is however very fragile and can be subjected to significant degradation after only tens of cycles in an aggressive environment, with H_2SO_4 as the electrolyte for example.

Table 2-1 : Diffusion constant of ionic species for WO_3 thin films prepared by different techniques.

Technique	Ion	D (cm²/s)
Evaporation	H^+	$10^{-10} - 2.5 \times 10^{-7}$
	Li^+	$1.5 \times 10^{-12} - 5 \times 10^{-9}$
	Na^+	$6 \times 10^{-20} - 1.8 \times 10^{-16}$
Sputtering	Li^+	10^{-11}
Sol-gel	Li^+	$5 \times 10^{-12} - 3 \times 10^{-11}$

Such systems can also be equipped with ion sources which allow for a controlled ion bombardment of the growing film's surface. While of use for etching and cleaning, another advantage is ion-assist, which offers a greater control over the microstructure of the growing film. The effect is very similar to what happens when substrate biasing is introduced during sputtering, as will be discussed in Section 2.3.3.

Ion assist and GLAD can also be combined to achieve interesting properties by both increasing the amount of porosity with a high deposition angle and densifying the resulting columns with high energy bombardment, thus improving the durability of WO_3 whilst maintaining performance. This approach is also under investigation in our research group and the subject of another master's thesis.

2.3.2 Sol-gel

The sol-gel process is mostly used for producing metal-oxides from a colloidal solution (the *sol)* that transforms into an integrated network (the *gel*). The network can be constituted of discrete particles or polymer chains. This is a wet chemical process and therefore very different from vacuum-based PVD techniques, but still of interest to us because of the possibility to assemble crystalline nanoparticles of WO_3 in an organized, porous network as mentioned in Section 2.2.5.2.

A tungsten precursor is first dissolved in a proper solution, WCl_6 in ethanol for example, then spin-coated and dried into an amorphous layer with a controlled microstructure. The material is then annealed at high temperature, crystallizing the tungsten oxide particles present in the network into a film that, if done correctly, will maintain its form [32], [33] (see Figure 2.8)

This evaporation-induced self-assembly can provide a three-dimensional mesoporosity, which is beneficial for cation insertion and thus the coloration process. The ion's diffusion path length is shorter, and can consequently move more easily in the WO_3 matrix. On top of that, the degree of crystallinity of the particles can be adjusted with the annealing procedure and the size of the nanoparticles controlled during the initial growth process [32].

While this method grants unprecedented control over the size, crystallinity and spacing of WO_3 nanoparticles, allowing for the formation of a 3-D framework suited to an application's needs, it was not investigated in the present project for several reasons. Firstly, the expertise of the FCSEL lies in the field of vacuum-based deposition technology, meaning that developing a completely

new sol-gel methodology would have been required. While this could have been surmounted, the same argument holds for our industrial partners who also prefer PVD-oriented processes. Finally, and perhaps the most compelling argument is that this method is much more complex, from the formation of the WO_3 particles to the many subsequent sol-gel steps, especially from an industrial standpoint. Translating such a process to a large-scale production would present inherent limitations, a major drawback compared to the one-step solution we developed via ion-assisted sputtering.

2.3.3 Sputtering

As was the case with e-beam evaporation, sputtering is a PVD technique but instead of vaporizing a sample with accelerated electrons, it relies on the momentum transfer from impacting ions. In its most simple form, DC (direct current) sputtering, a potential is applied between a target, the cathode, and the substrate holder which serves as the anode. Electrons present in the chamber are accelerated towards the anode and ionize a working gas inserted into the chamber, usually argon because it is the cheapest of the noble (inert) gases and easy to ionize. This generates a plasma, a neutral cloud of positively charged ions, electrons, neutrals and radicals. The positive ions are then accelerated towards the cathode and impact the target, transferring their energy. If the energy is high enough (another reason why argon, a relatively heavy noble gas, is used), meaning higher than the binding energy of the target material, atoms are ejected from it. The atoms then travel through the chamber and condense onto surfaces, including the sample held above (see Figure 2.9) [15].
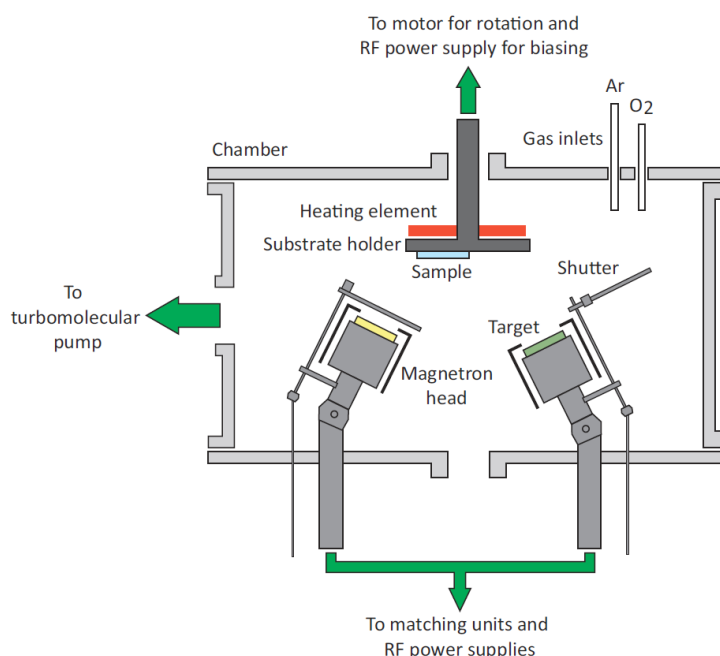
Figure 2.9 Schematic representation of a chamber used for radio-frequency magnetron sputtering. Taken from [15].

Note that the schematic depicted in Figure 2.9 is for RF (radio-frequency) sputtering rather than DC. While they look similar, the difference resides in the type of power supply employed. The reason to use RF is that direct current sputtering may only be implemented with conductive targets; otherwise, it becomes impossible to sustain the discharge. RF sputtering was introduced to circumvent this problem: by applying a 13.56 MHz signal, the plasma frequency is increased, and a current can be applied on a dielectric target, with the additional advantage of an easier to sustain discharge thanks to higher discharge energy.

Since electrons have a much higher mobility than the ions, they can more easily follow the rapid change of polarity and the two electrodes appear negatively charged relative to the plasma. The equivalent circuit is two series of capacitors, one representing the target's sheath and the other the substrate stage, connected to the chamber walls, baseplates, ground, etc. Since the capacitive reactance is inversely proportional to the area of the capacitor, the smaller sheath will see a much larger negative voltage. This ensures that most of the sputtering will occur at the target and not at the substrate [34].

Sputtering can also be done in a reactive environment, in which case gases such as O_2, N_2 and H_2 are also introduced in the chamber. The reaction is then more complex, as target poisoning can occur, but allows for a greater control over the stoichiometry of the deposited film. It is also necessary if one wants to prepare an oxide from a metallic target, for example WO_3 from W. In this project, both DC and RF methods were used and led to very similar results once the proper oxygen balance for sputtering from a pure W target was found.

The cathode in RF sputtering systems is also usually implemented as a magnetron, which consists of permanent magnets placed under the target. By superimposing a magnetic field to the electric field, a Lorentz force makes the electrons travel in a helical motion towards the target. This results in plasma confinement, increasing the ionization probability and therefore the plasma density. This correspondingly increases sputtering and, in turn, the deposition rate. Thanks to these higher rates, typically an order of magnitude higher than conventional sputtering, magnetron sputtering is the most widely employed commercial method [34].

2.3.3.1   Control of film properties through the control of deposition conditions

There are several parameters that can be adjusted in an RF sputtering system. The first one is the power applied between to the electrodes, which mainly controls the deposition rate by increasing the current density. A higher potential also means more acceleration for the ions in the plasma before they impact the target. This results in a greater momentum transfer, more atoms sputtered and a higher energy for these atoms. The growth of the film will be affected since more energy allows the atom to diffuse on the surface more easily, to reach a more ordered structure and usually producing denser films.

 The power required varies between different materials and is dependent on the size of the target which is used, so it is more accurate to speak in terms of power density. One must also be careful not to damage the target by applying a potential that is too high. Because of thermal shock being a concern with dielectric targets, a ramping period is usually recommended. The way the power is applied also has importance. Pulsed-DC sputtering, for example, is used to minimize arcing and improve deposition rates for reactive sputtering of some dielectric materials like silica and alumina. Another method, high power impulse magnetron sputtering (HiPIMS), uses short bursts of very high-power density to achieve denser materials with improved adhesion.

A second way of controlling the deposition process is by changing which gases are injected into the system. As previously mentioned, argon is usually the favored gas for the major part of the mixture because it is inert, meaning that the target material won't be chemically affected by the sputtering process, relatively heavy for more efficient sputtering and cheap enough to be used in large quantities. Added to it can be reactive gases; oxygen and nitrogen are obviously required to make oxides and nitrates. In the case of WO_3, by changing the O_2-to-Ar ratio, the composition of the deposited film can be adjusted to be slightly sub or over stoichiometric. This is especially true if one sputters from a pure W target instead of WO_3 and can be an interesting way to improve the performance of the material. Indeed, some studies have shown that slightly sub-stoichiometric tungsten oxide can result in significant changes of the optical properties, such as absorption bands appearing in the near-IR and a shift of the band gap [35].

In the case of electrochromic devices, the addition of hydrogen to the gas mixture can result in pre-insertion of cations in the films to be used for the coloration phenomenon. This can be done either during the deposition of WO_3 or its anodic counterpart, for example, NiO [16]. This opens the possibility of fabricating fully-functional devices without the need to break the vacuum to chemically insert the ions in one of the layers. There are important advantages associated with this, namely production speed on an industrial line, better control over the conditions in the system, and less risk of contaminating the sample before the process is complete, which can otherwise result in short-circuiting, reduced coloration speed and lifetime, or even a non-functional device.

Another manner to modify the properties of a prepared film is to dope it by co-sputtering another material, which will result in irregularities in the lattice, defects and changes of properties. One example of co-sputtering being of interest for WO_3 is the addition of Mo, which can improve durability and grant a more neutral color. Other multicomponent films include binary oxides with vanadium, tungsten oxyfluorides and tungsten-metal composites, in an effort to improve the coloration dynamics, achieve higher deposition rates or produce multi-color films [16]. It is also possible to heat the system during deposition, which will increase the energy and mobility of the atoms on the substrate. By doing so, it is possible to increase the order and eventually crystallize the material if a high enough temperature is reached. A study by Kim *et al.* has also shown that better EC properties can be achieved with moderate heating by affecting the size of nanocrystals in the material [36].

The main parameter that can affect deposition, and especially the microstructure, is the pressure in the system, which needs to be very accurately controlled. One might think that more particles means a higher plasma density and an effect akin to increasing the potential, but it is the opposite. Since the sputtered atoms need to travel to the substrate, the more particles are in the way, the more collisions will occur. Each of these collisions reduces the energy of the incident matter and has a chance to stop or divert it entirely (mean free path reduction - shadowing effects due to the loss of directionality). In fact, the higher the pressure, the more porous the resulting thin film and the slower the deposition rates.

Since a certain level of porosity is required for the proper functioning of WO_3 as an EC material, previous studies have shown that 10-20 mTorr is the ideal deposition pressure range for amorphous tungsten oxide films [11], [12]. Lowering the pressure increases the durability but quickly reduces the film's EC performance and conversely, increasing the pressure yields improvements in performance at the detriment of durability; therefore, a compromise must be made between these two criteria.

Ideally, we would like to be able to profit from an increased material density (and durability) as well as deposition speed which comes with using a lower pressure. The question then becomes, how can we introduce voids into the material to maintain adequate ion diffusion without increasing the pressure and sacrificing durability? This is where substrate biasing comes in.

2.3.3.2 Impact of ion bombardment on the microstructure

During the section on e-beam evaporation, there was mention of using ion assist as a means to influence the microstructure of the growing film. Although an ion gun can also be added to a regular sputtering system, another way to achieve a similar effect without having to is to add a generator that will apply a potential between the substrate holder and the grounded frame of the deposition chamber. This will accelerate ions from the gas mixture, resulting in ion bombardment of the growing film, the energy being tuned by the applied potential. The general effect of ion bombardment depending on the level of energy and flux of ions is very well represented in the modified structure zone model by A. Anders (see Figure 2.10) [37].
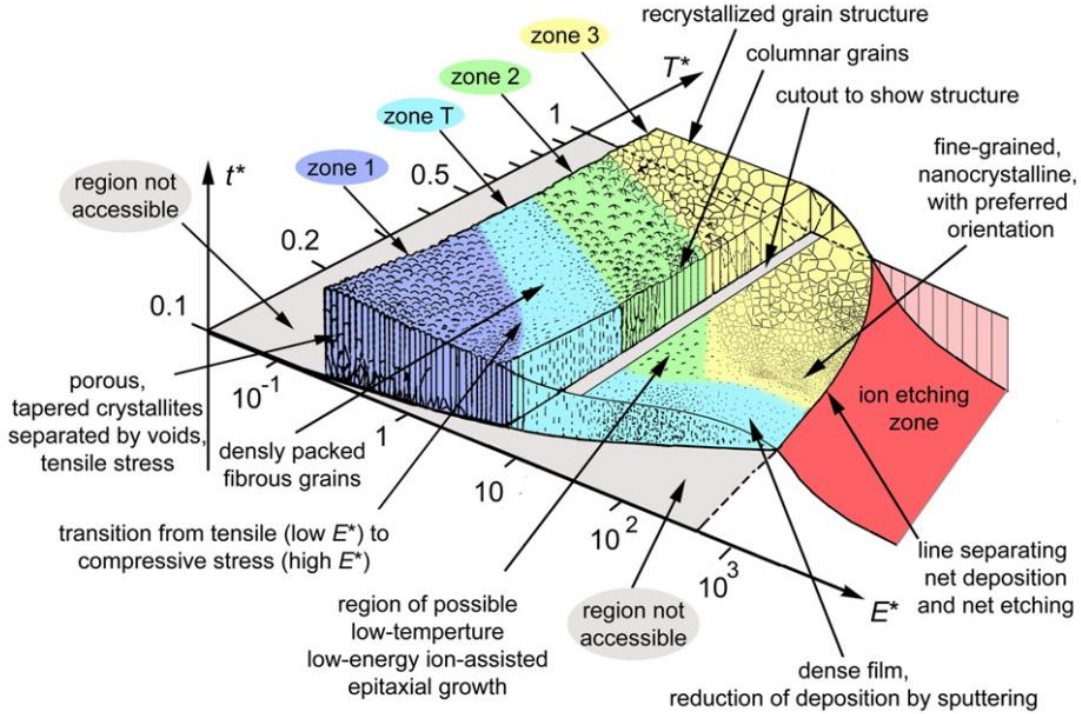
Figure 2.10: Structure zone diagram applicable to energetic deposition. Values are for orientation only – the actual values depend on the material and many other conditions and therefore the reader should avoid reading specific values or predictions. Taken from [37].

The model also shows the effects of temperature and pressure on growth with the E^* axis representing the energy flux (energy from the bias acceleration). It shows that increasing the pressure results in a more porous structure with an increasing amount of voids separating the crystallites, while a temperature increase will make the material transition into a densely packed fibrous grain transition region, followed by columnar grains and finally a recrystallized structure. By reaching high enough ion flux and ion energies, the material transitions in a similar way as when increasing the temperature but finer grained, with nanocrystallization, densification and resputtering occurring. To quantify the effect of ion bombardment, the energy deposited per particle given by equation 4 is useful:

$$E_p \sim E_i \, \frac{\Phi_i}{\Phi_n} \tag{4}$$

where E_i is the energy per particle, Φ_i is the ion flux and Φ_n is the flux of condensing particles. We can see that not only the energy but also the flux of particles has an impact. Substrate biasing, however, only gives control over the former while changing the pressure in the chamber will also have an impact on the result. Figure 2.11 gives an overview of the effect of increasing one parameter or the other [38].
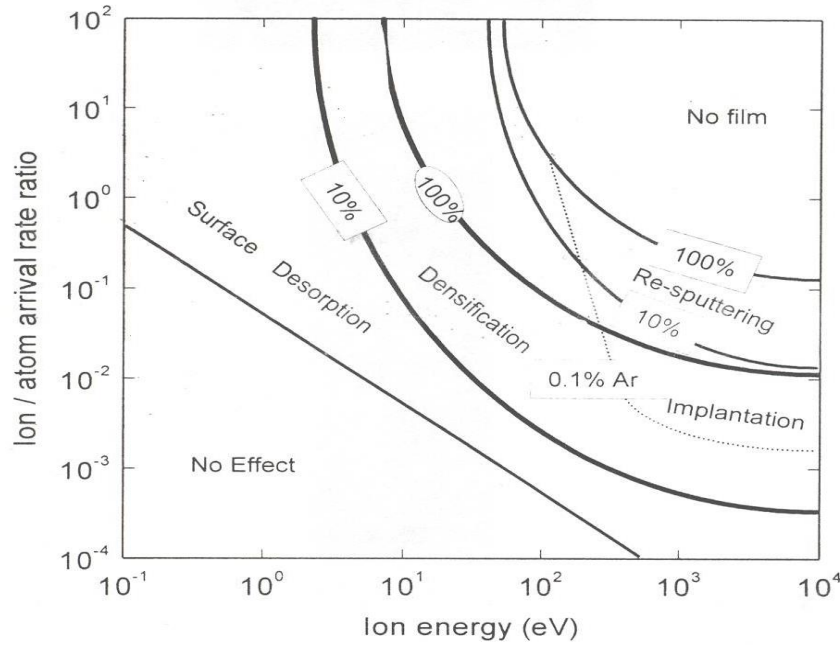
Figure 2.11: Critical ion energy and ion flux and their effects on the film's growth. Taken from [38].

Many studies on the effect of biasing on different materials have been realized over the years. A study on titanium dioxide concludes that strong modification the film's microstructure can be expected with substrate biasing, with metallic materials being much more sensitive to ion bombardment than oxides [13]. Another work showed that the ion bombardment could remove part of the oxygen through preferential resputtering and strongly affect the crystallographic structure of Cu_2O films [39]. A study of the effect on WO_3 up to -150 V indicated a reduced nucleation energy, variations of the morphology and changes to the absorption behavior, with the appearance of a monoclinic phase of WO_3 in an amorphous matrix; however, no mention of the EC properties of their films was made [40]. The effect of substrate biasing on Ta_2O_5 was reported to increase the packing density and refractive index up to -150 V, then decreased both of these parameters at higher

voltages possibly due to argon incorporation and the creation of oxygen deficiencies [41]. Finally, an earlier paper exposed that the void network structure in WO_3 controls its electrochromic behavior and can be controlled primarily through ion bombardment of the growing film. More specifically, the largest voids at the surface of a film are the main vector for proton injection and thus by controlling the mobility of atoms during growth, the hydrogen transport should also be controllable [42].

Putting all this together, we can understand the following: at lower energies, ion bombardment densifies the WO_3 layer and reduces the amount of porosity present in the network, decreasing the electrochromic performance. Then, at higher energies the morphological effects change, resputtering results in a possibly more porous material, defects such as argon trapping and oxygen deficiencies are created and even crystallinity or stoichiometry modification can occur. These effects can be exploited to create a structure with a larger void network favorable for proton intercalation. However, to the best of my knowledge no research on WO_3 with substrate biasing at a potential much higher than -150 V has been done, much less up to -500 V.

Chapter 4 of this thesis shows our findings regarding the impact of ion bombardment at very high energies on the microstructure of a WO_3 thin film and the associated changes in EC performance. Before that, however, chapter 3 will expose how we produced and analysed the EC films.

CHAPTER 3   METHODOLOGY

This chapter outlines the various experimental procedures undertaken during the present project going from sample preparation to characterization. The employed deposition technique was bias-assisted RF magnetron sputtering. Once produced, the samples were first characterized by variable angle spectroscopic ellipsometry and spectrophotometry (reflection and transmission). Their electrochromic performance was then quantified by cyclic voltammetry measurements. Finally, to establish a link between the microstructure of the produced films and their EC activity, a series of physical characterization tests was implemented: AFM (atomic force microscopy) to measure roughness and observe the general topography before and after CV cycling, Raman spectroscopy to evaluate crystallinity, Rutherford back-scattering for composition and finally SEM (scanning electron microscopy) and TEM (transmission electron microscopy) to observe the microstructure and ascertain the presence of crystallinity in the biased samples.

3.1   Bias assisted RF magnetron sputtering

Having previously described the theory behind RF sputtering in Section 2.3.3, we will now focus on the exact deposition conditions used during this project. Preliminary depositions and observations were performed in a homemade RF magnetron sputtering system equipped with four two-inch magnetrons. As previously mentioned in the introduction, the initial objective of this research was to create a dense WO_3 layer which could act as an ion barrier without impeding electron diffusion. To do so, the pressure was lowered from our usual 20 mTorr down to 5 mTorr with the addition of increasingly high values of substrate biasing. Having observed and discovered an unexpected increase in EC activity for samples deposited at a bias voltage of -410 V (highest attainable value), it was decided to pursue this research in a Kurt J. Lesker fully automated deposition system equipped with four three-inch magnetrons which allowed us to lower the deposition pressure to 1 mTorr and increase the intensity of the bias voltage to -525 V, conditions that did not result in a stable discharge in the smaller homemade chamber.

The deposition conditions for the WO_3 layers can be found in Table 3-1. The base pressure in the system was lower than 9×10^{-8} Torr prior to inserting the samples through a load-lock system. Argon and oxygen were introduced through mass-flow controllers at a 20% O_2/Ar ratio. The discharge power was kept constant for all samples at 438 W (9.6 W/cm^2).

Table 3-1: Deposition parameters for WO$_3$ thin films prepared by RF magnetron sputtering.

Sample	Pressure (mTorr)	Substrate bias (V)	Target Power (W)	Target voltage (V)	Layer thickness (nm)	Deposition time (s)	Deposition rate (Å/s)
1	20	0	438	107	136	5500	0.25
2	1	0	438	200	133	875	1.5
3	1	-525	438	201	137	1050	1.3

Having tested various deposition conditions to confirm that the CMS-18 also gave comparable results, multiple samples were then prepared to verify the reproducibility of the samples, and on different substrates, mainly Si (100) crystalline wafers, B270 glass and ITO (indium-tin-oxide) covered glass slides from Delta Technologies with a sheet resistance of 30 Ω/□ for the various characterization techniques. Two additional series of samples, one at 1 mTorr without bias and one at 20 mTorr without bias, were also prepared for comparison purposes. The glass substrates were precleaned with a soap-water mixture, then all substrates were cleaned with isopropanol in an ultrasound bath, rinsed with deionized water and finally dried in nitrogen.

Although samples deposited at 20 mTorr with high substrate bias voltages were also investigated, they offered poor EC performance and as such were not investigated further. In parallel with the main work on biasing, some of my efforts were also dedicated to developing an all solid-state electrochromic device. As this work does not directly relate to the main body of this project, it will only be discussed further in Chapter 5.

3.2   Optical properties characterization

As the development of high-performance WO$_3$ layers was done in the context of smart windows, ensuring good optical properties was paramount; i.e. a high transparency in the visible and NIR spectrum in the bleached state and relatively low refractive index indicative of the presence of porosity. The first step after any deposition was therefore to verify the optical properties of the samples, first by ellipsometry and then by spectrophotometry when additional information on the presence of absorption or for precise assessment of the reflectance was required.

3.2.1 Spectroscopic ellipsometry

Variable angle spectroscopic ellipsometry (VASE) is a non-intrusive indirect optical characterization technique which offers a significant amount of information following a single measurement. Indeed, through the elaboration of an optical model, information on the presence of surface roughness, the thickness of the layer and dispersion curves (*n* and *k*) can all be obtained. Pushing the model further may also impart information on the presence of anisotropy or growth gradients in a sample. The technique also allows differentiation and characterization of multiple layers in a film, provided sufficient information on the individual film is already known.

Ellipsometry relies on the change in polarization of an incident light beam of known polarization after reflection on the surface of a sample. The name of the technique arises from the fact, that in most instances, the resulting reflected beam is usually elliptically polarized (see Figure 3.1, from [43]) .
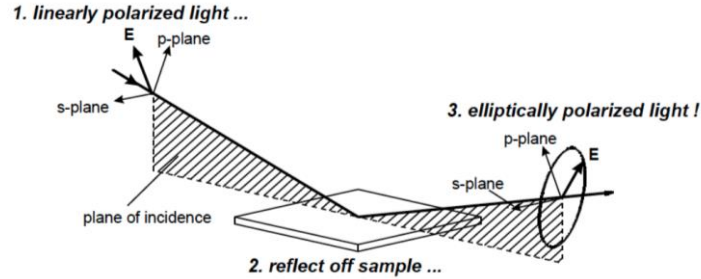
Figure 3.1: Interaction between a light beam and a surface. Elliptical polarization occurs after reflection on a thin film [43].

After interaction with the sample, both *s* (perpendicular) and *p* (parallel) polarizations will see their phase and amplitude change. This difference is quantified by the ellipsometric parameters Ψ and Δ, which can be obtained through the following equation:

$$\tan(\Psi)\, e^{i\Delta} = \rho = -\frac{r_p}{r_s} \tag{1}$$

where r_p and r_s are the complex Fresnel coefficients for the *p* and *s* polarizations respectively and ρ is a ratio which gives information on the phase difference (Δ) and amplitude ratio (Ψ) of between both polarizations.

The instrument used for those measurements was an RC2 ellipsometer equipped with two rotating compensators fabricated by the *J.A. Woollam Co.* Measurements were performed at four angles of incidence (45°, 55°, 65°, 75°) from 200 nm to 1700 nm. The ellipsometric experimental results are then compared to an optical model based on the use of Tauc-Lorentz, Gaussian or other oscillators using the *CompleteEase* software, also supplied by J.A. Woollam Co. By refining the model until its optical response matches the measurement, we can expect an accurate assessment of the physical properties of the sample (thickness, optical properties, etc.) provided the model is accurate. This optimization step is based on the mean squared error (MSE) minimization and will be more likely to succeed if the initial parameters are close to reality, meaning that having prior information on the thin film will help with the modelling.

For WO_3 layers, a Tauc-Lorentz oscillator is often sufficient to implement the model, but this was not the case for the biased samples. It is the TEM measurements that revealed that the deposited layer had two major distinct phases (see Chapter 4) prompting us to implement a two-layer model

Ellipsometry can also be used to evaluate the packing density of thin films. By extracting the refractive index value at 550 nm and comparing it with the bulk value of the material (typically 2.5 for WO_3 [16]) the Lorentz-Lorenz effective medium approximation (EMA) allows one to calculate the packing density [15]:

$$P = \frac{n_f^2 - 1}{n_f^2 + 2} \frac{n_b^2 + 2}{n_b^2 - 1} \tag{2}$$

where n_f and n_b are the thin film and bulk refractive indices of WO_3 respectively.

It is useful to evaluate how dense the material is in comparison to the 20 mTorr and non-biased 1 mTorr samples and see how this affects the EC performance.

3.2.2 Spectrophotometry

Additional transmission and reflection measurements over the 250-1700 nm region were obtained with Agilent Technologies' Cary 7000 spectrophotometer equipped with a Universal Measurement Accessory (UMA) allowing for multi-angle measurements without having to manually reposition the sample as the detector moves around the sample. While these could be obtained or derived from

ellipsometric modelling, direct measurements allowed for a greater precision. This method was especially useful to observe the loss of transmission after EC coloration of the samples and whether it was based on an absorption or reflection modulation and, therefore, observe the potential presence of more reflective crystalline phases in the samples.

3.3 Electrochemical characterization

3.3.1 Cyclic voltammetry

Cyclic voltammetry consists in the continuous switching of a potential between two values at a specific scan rate, allowing to obtain the chemical signature of a sample going from its colored to
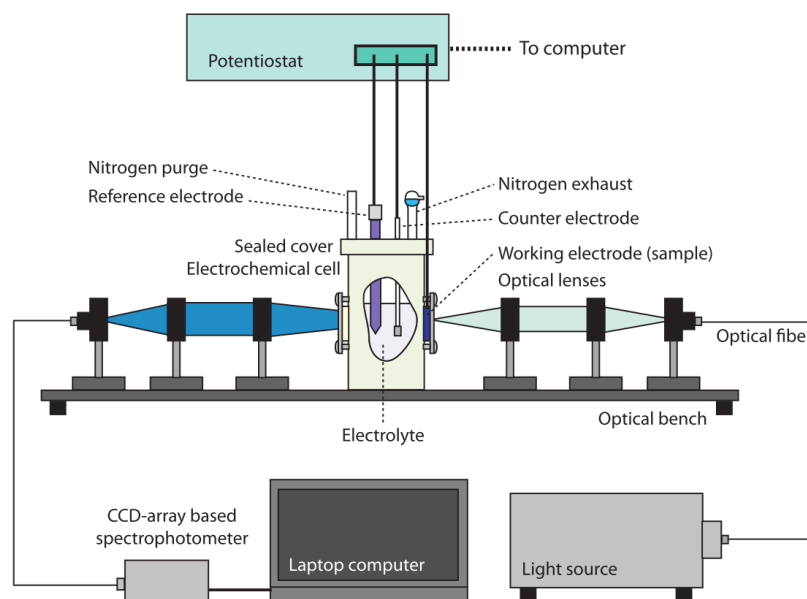
Figure 3.2: Electrochemical measurement setup with combined in situ transmission measurements [15].

its bleached state and back. The sample is put in contact with an electrolyte solution through a window in an electrochemical cell, with a second window on the opposite side for transmission measurements. The cell is filled with an electrolyte, in our case a 0.1 M H_2SO4- solution chosen for its ability to supply substantial amounts of H^+ ions for intercalation. A three-electrode configuration, the working electrode (ITO under the sample), counter electrode (graphite) and

reference electrode (standard calomel electrode) is controlled by a potentiostat (in this case the *Autolab PGSTAT302N* from Metrohm Autolab). For a representation of the experimental setup, see Figure 3.2 (from [15]).

A potential ramp between two set values of -0.5 V and 1.2 V was applied back and forth between the working and counter electrodes for a specified number of cycles at a 25 mV/s scan rate, with an initial 30 s bleaching period. The generated current is monitored to obtain a voltammetric curve. A typical example for a WO_3 sample prepared at 20 mTorr is shown in Figure 3.3.
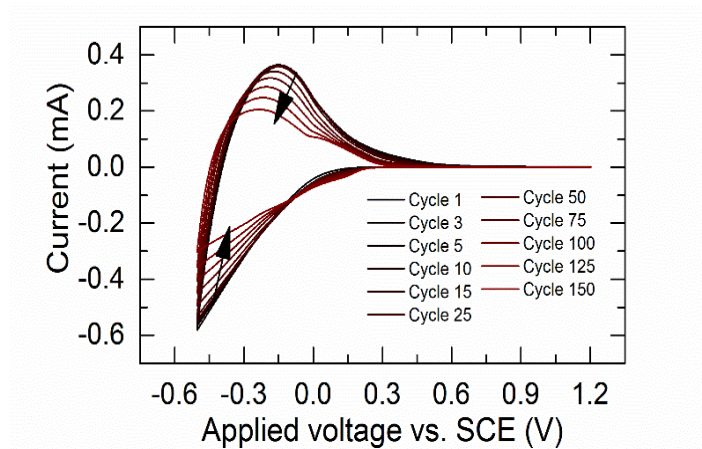
Figure 3.3: Typical "duck-shaped" curve observed when coloring and bleaching an amorphous WO_3 sample. The data corresponds to Figure 1 of Chapter 4.

The bottom region corresponds to the coloration phase of WO_3 (cathodic current), in which peaks can be identified in the right conditions (low scan-rate, for example) and serve as a means to identify different W reduction states and, possibly, the presence of crystallinity in the layer (see Figure 3.4, from [25]).

The top part is the bleaching phase (anodic current) and the maximum value is defined as the anodic peak current i_p. From this value, provided the reaction is fully reversible one can calculate the diffusion coefficient of ions with the Randles-Sevčik equation, used to describe the effect of the scan rate on peak current (based on the Nernst equation for redox events):

$$i_p = 0.4463 n_e F A c_s \sqrt{\frac{n_e F v D_i}{RT}} \tag{3}$$

where n_e is the number of electrons taking part in the reaction, F is the Faraday constant (C/mol), A the working electrode area (cm^2), c_s the solution concentration (mol/cm^3), v the scan rate (V/s), R the universal gas constant (J/mol·K), D_i the ion diffusion coefficient (cm/s) and T the ambient temperature (K) [15].
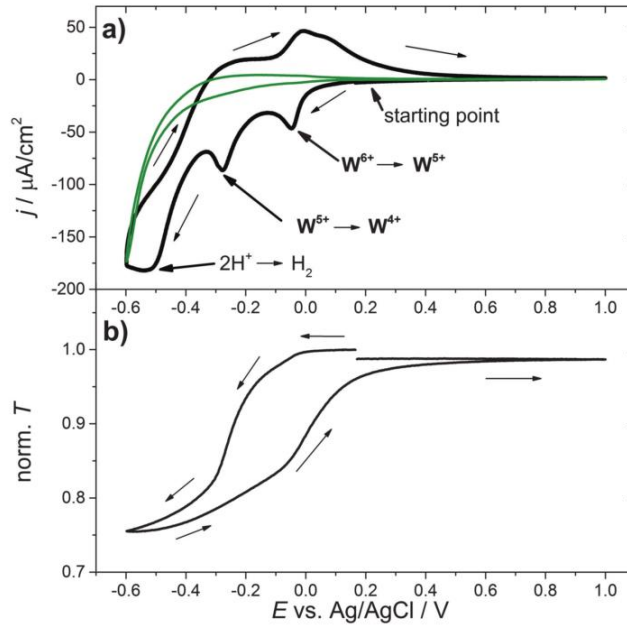
Figure 3.4: (a) Cyclic voltammogram of a WO3 film in a 0.1 M H2SO4 in H_2O electrolyte with a scan rate of 1 mV s^{-1}. The green curve shows the same measurement for the substrate alone. (b) Corresponding transmission characteristics during hydrogen insertion recorded for a spectral window of 633 nm +/- 15 nm. Norm. T denotes the transmission T at the center wavelength 633 nm normalized to the corresponding transmission T_0 at the beginning of the experiment [25].

Knowing the scan rate, the increments in potential can be converted into time increments and by multiplying the current by this value, the inserted or extracted charge can be calculated. Doing so for all negative current values returns the total inserted charge, while the positive currents provide the extracted charge. Their ratio provides information on how much charge remains trapped after a coloration cycle or is lost to side reactions, which in turn is a good indicator of the evolution of the degradation in a coating.

The H_2SO_4 solution is also a relatively aggressive environment which will quickly deteriorate amorphous WO_3 samples, allowing to rapidly assess the durability of the material by looking at its degradation over time.

3.3.2 *In situ* transmission

The electrochemical setup also allows for transmission measurements in parallel with the coloration and bleaching cycles using a tec5 MultiSpec Pro spectrophotometer. The acquisition was performed at 550 nm every 500 ms. As the baseline measurement was performed with the sample in place, the bleached state of a sample corresponds to 100%. This is not a problem, as calculating the coloration efficiency (CE) relies on the ratio of transmission variation using the following formula:

$$CE = \frac{\ln\left(\frac{T_b}{T_c}\right)}{Q/A} \tag{4}$$

where T_b and T_c are the transmission in the bleached and colored states respectively, Q is the total inserted charge and A is the colored surface's area.

Indeed, the CE is the most commonly used parameter to evaluate how well an electrochromic layer performs and when combined with the charge extraction ratio and the ion diffusion coefficient, give a good indication of how well this performance will be maintained over multiple cycles.

Typical 20 mTorr amorphous WO_3 thin films intercalated with H+ ions are typically considered to have good CE values when around 40-and normally start showing signs of degradation after only 20 cycles (see Chapter 4). For this reason, Li ions are often used instead of H+ ions due to a reduced amount of damaging side-reactions. This however requires a more sophisticated setup which purges any trace of water to avoid contamination. Evaluating durability being one of my objectives, the degradation was not seen as a problem and H^+ insertion was favored.

3.4 Physical characterization

Having measured the optical and EC properties of our WO_3 films, additional tests were required to find an explanation for the increased performance. The answer was sure to lie in the microstructure of the films which was thus investigated using a series of well-known characterization techniques

which are briefly outlined below.

3.4.1 Atomic force microscopy

AFM is a high-resolution (nanometer-scale) type of scanning probe microscopy. A cantilever equipped with a nanometer-sized tip is raster scanned above the surface of a sample to measure the force of the tip-surface interaction.

Force measurement relies on quantifying the interaction between the probe and the material, measuring the phase and amplitude of the cantilever's oscillations as it scans the surface, to return the mechanical properties of the sample, Young's modulus and stiffness for example. In imaging mode, a laser is reflected on the top of the cantilever onto a reference grid to measure the height of the probe as it scans across the sample. The gathered information can then be used to build a three-dimensional map of the surface one line at a time.

This technique being relatively inexpensive, it was the first used to see if any structural modification occurred following the application of biasing. It was also used to evaluate the amount of degradation after cycling in H_2SO_4 by measuring the surface roughness, overall topography and integrated surface area difference (ISAD) before and after the test.

3.4.2 Raman spectroscopy

Raman spectroscopy is a technique based on the excitation of vibrational and rotational modes in a material, complementary to infrared spectroscopy. A laser beam illuminates a sample and the radiation coming from it is collected according to its energy. When inelastic, or Raman, scattering occurs the re-emitted beam will be energy shifted, either negatively (Stokes) or positively (anti-Stokes). The energy of these shifts can be associated with the type of chemical bond and therefore give information on the chemical composition of the analyzed sample.

Since the collected information is linked to chemical bonds, it is also possible to use this technique to evaluate the crystallinity in WO_3 samples. W-O-W type bonds can be measured as a Raman shift around 719 cm^{-1}, 807 cm^{-1} and the W=O bond at 960 cm^{-1}. A decrease of the 807 cm^{-1} peak's FWHM (full width at half maximum) reflects an improvement in the structural order of the material and therefore crystallinity, while the ratio of the two stretching modes W=O/W-O can be used to evaluate the degree of crystallinity. Figure 3.5 shows how heating a sample results in a reduction

of the 807 cm^{-1} peak [44].
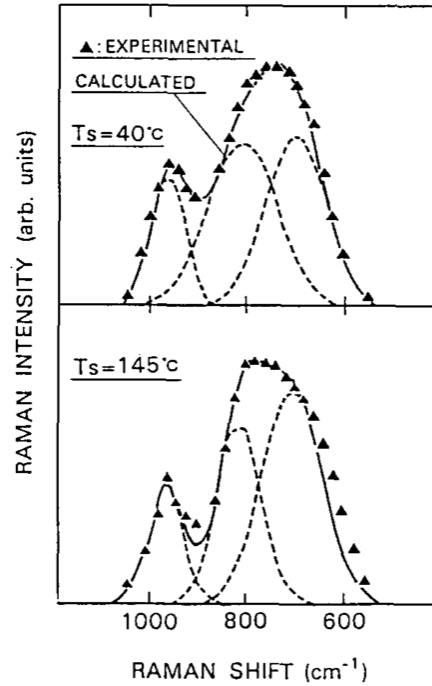
Figure 3.5: Deconvolution analysis of the Raman spectra of a-WO 3 films. Solid lines show calculated curves which were obtained by the synthesis of three gaussian components. Triangles show the observed spectra [44].

3.4.3 Rutherford back-scattering

Rutherford back-scattering spectroscopy (RBS) uses a beam of high energy particles (2 MeV of He$^+$ the present case) to probe the composition profile of a sample. By measuring the energy and number of backscattered ions, which are the result of elastic collisions with the nuclei of atoms in the sample, it is possible to infer the mass of the nucleus responsible for the scattering. The concentration of elements at each depth of the film can be determined as a deeper measurement will result in a broader peak.

Hydrogen atoms being too light to measure by RBS, elastic recoil detection (ERD) is used as a complementary method. With the same setup, these atoms are expelled from the film and collected

via an appropriate detector. Figure 3.6 shows the setup used in this case (from [15]).
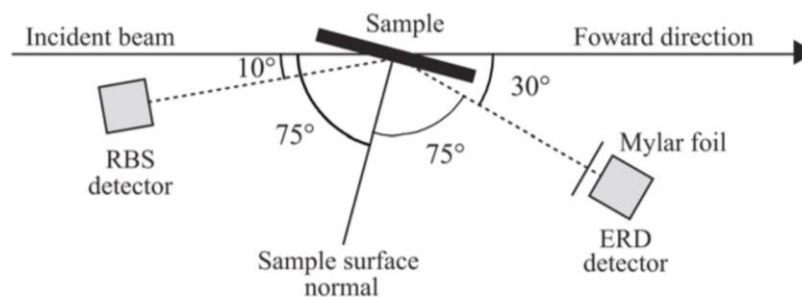
Figure 3.6: Setup used for RBS and ERD measurements in the present thesis. Taken from [15].

Since this technique can have difficulties differentiating WO_3's chemically bonded oxygen from the atoms of water absorbed in the film, it is not accurate for determining the stoichiometry of our films. It was mostly used to evaluate the packing density of the material to corroborate the results obtained from the ellipsometric modelling. It was also used to measure the change in the concentration of argon trapped in the layers as a consequence of biasing, which can be an indicator of increased porosity.

3.4.4 Scanning electron microscopy

Scanning electron microscopy (SEM) is a type of microscopy that allows for the imaging of very small structures in a non-destructive manner by scanning an electron beam over surface. Secondary electrons of low energy (< 50 eV) resulting from inelastic collisions are then collected and analyzed. Depending on the angle at which the beam hits the surface, more (at higher angle) or less of these electrons are emitted resulting in a contrasting image which allows one to obtain information on the topography of the sample. As the secondary electrons cannot escape from more than a few nanometers of material, only the surface of a sample can be imaged. Their emission is also sensitive to the atomic number of the scattering atom, meaning that heavier atoms will appear brighter allowing to identify differences in composition.

Backscattered electrons are also emitted from the interaction between the electron beam and the nuclei. Backscattering, like secondary electron emission, is influenced by atomic weight. Collecting them instead results in a more chemically sensitive image than with secondary electrons

but the topographical information is mostly lost. The two measurements are often used in combination to gain as much information as possible. Finally, X-rays are also produced during the interaction and energy-dispersive X-ray spectroscopy (EDX) can be used to analyze composition. The instrument used for this project was a JEOL JSM-7600F and WO_3 layers deposited on Si wafers were cleaved to allow for a view of the cross-section.

3.4.5 Transmission electron microscopy

In order to confirm without any remaining doubt the presence of crystallinity in the biased samples, measurements were also made with a transmission electron microscope (JEOL JEM-2100F). This method consists in exposing a sample to an electron beam and collecting the electrons that pass through it to form an image. In mass-thickness contrast mode, heavier atoms scatter the electrons at a higher angle and appear darker allowing for chemical identification. In diffraction contrast mode, diffraction occurs due to the crystalline structures in the sample and a lot of crystallographic information can be gained. Due to the strong interaction between electrons and solid matter, only very thin samples (< 100 nm) can be properly analyzed; otherwise, insufficient electrons can escape.

While this method usually implies a very costly sample preparation step with focused ion beam (FIB) etching, an alternative preparation technique consists in generating powder by scratching the film's surface using a razor blade and transferring the resulting powder onto a TEM sample support mesh. This process essentially destroys any information related to the microstructure of the film but still allows for the observation of crystallinity in a sample as well as identification of the type of lattice.

Following the confirmation of the presence of crystallinity in our biased samples, additional TEM measurements following a costlier FIB sample preparation were performed to gain structural information

CHAPTER 4   ARTICLE 1: HIGHLY DURABLE ELECTROCHROMIC TUNGSTEN OXIDE THIN FILMS PREPARED BY HIGH RATE BIAS-ENHANCED SPUTTER DEPOSITION

F. Blanchard[a], B. Baloukas[a] and L. Martinu[a]

[a] Department of Physics Engineering, Polytechnique Montréal, Montreal H3T1J4, Canada

4.1 Foreword

This chapter consists of the article as it was submitted for publication to the journal *Applied Materials Today*. The work was realized using the methodolody outlined in Chapter 3 and consists of our main findings regarding the use of susbtrate biasing to enhance the performance of electrochromic WO_3 layers deposited with RF magnetron sputtering.

4.2 Abstract

Electrochromic (EC) materials are of interest for applications such as smart windows for increased energy efficiency, but their long-term durability remains an issue for widespread implementation and commercialization. In the present work, we compare traditional radio frequency (RF) magnetron-sputtered porous WO_3 films produced at high pressures (20 mTorr) with films deposited at lower pressures (1 mTorr) under energetic ion bombardment due to intense substrate biasing. Our results show that above a specific threshold substrate bias voltage of ~400 V, the films exhibit not only comparable EC properties and coloration efficiencies with their higher-pressure porous conterparts, but also an exceptional long term durability in a 0.1 M H_2SO_4 electrolyte, while being deposited five times faster. The observed performance increase is ascribed to the high energy ion bombardement induced effects leading to the formation of a nanocrystalline WO_3 matrix, while simultaneously generating the necessary porous microstructure for ionic diffusion. This novel fabrication approach is believed to pave the way toward more cost-effective fabrication of highly durable EC devices and enhancement of their application in different sectors.

4.3   Introduction

The building sector is known for its high energy consumption which represents 30-40 % of the world's primary energy expenditure [3]. Operational costs, such as heating, cooling,

ventilation and lighting account for the better part of this consumption, especially in older structures built under less stringent energy efficiency construction standards. Since windows are usually the weak link in a building's isolation [45], and considering modern architectural designs that often include whole glass facades, it becomes apparent that better insulating windows are a priority in order to control and reduce energy waste. There are, therefore, significant advantages both environmentally and economically in developing highly insulating windows.

Thin film technology represents a promising avenue, as it can be either applied directly onto glass during production, or on a polymer web which could then be retrofitted onto already pre-existing windows at correspondingly lower costs. A passive application of this technology based on the use of thin silver or transparent conductive oxide films, low-emissivity coatings, is already extensively implemented on the market [8]. A step forward are so-called electrochromic (EC) "smart" windows which integrate a WO_3 layer, the most extensively studied EC material for this kind of application [4],[5]. Both the characteristic change in optical properties upon the voltage-driven electron and ion insertion and the reversibility of the coloration process allow for direct control of the amount of visible and near-infrared light which can pass through a window. Going from passive to active in this manner makes it possible to achieve both a higher level of comfort for the user and a better control over energy expenditures.

Ensuring long-term durability of the EC material has been of major concern and the subject of multiple studies [4],[6] as it is obviously an important parameter for architectural and other applications. Studies have shown that the use of nanocrystalline WO_3 can solve the problem of chemical stability, whilst maintaining or improving its EC properties over amorphous films [33], [46]. However, the fabrication of such nanocrystalline films often requires multiple steps and is often reliant on chemically-based processes such as sol-gel or HWCVD (hot-wire chemical vapor deposition) making them harder to implement for large-scale industrial applications both from technical and environmental standpoints.

To satisfy the need for high durability and industrial scalability, in this work, we investigate a new single-step approach to fabricating EC WO_3. Specifically, we study the impact of applying negative substrate biasing during WO_3 RF sputtering, typically known to lead to densification [13] and thus, a priori, generally detrimental to EC materials. We show that this is indeed the case for films deposited at low pressure (1 mTorr) using low bias voltages (under 400 V). However, when surpassing a specific threshold voltage (> 400 V in the present case), the resulting films are shown to regain their EC activity and possess a surprisingly high long-term chemical durability. We compare the resulting thin films' EC performance to their non-biased counterparts and typical porous WO_3 films deposited at higher pressures (20 mTorr) by performing electrochemical ion insertion via cyclic voltammetry. We then perform an extensive structural and physical analyses of the samples, and demonstrate the formation of a porous amorphous/nanocrystalline microstructure responsible for the observed enhanced EC performance.

4.4 Materials and Methods

4.4.1 Sample deposition

Thin films of WO_3 were prepared by RF magnetron sputtering in a CMS-18 system acquired from Kurt J. Lesker and fitted with a 3-inch diameter target of WO_3 (99.9% purity, Kurt J. Lesker). The base pressure in the system was lower than 9 x 10^{-8} Torr prior to inserting the samples through a load-lock system. Argon and oxygen were introduced through mass-flow controllers at a 20% O_2/Ar ratio. The discharge power was kept constant for all samples at 438 W (9.6 W/cm^2). Substrates for electrochemical analyses consisted of 2.5 cm x 5 cm ITO-coated glass with a sheet resistance of 30 $\Omega/\square$ (Delta Technologies) and were precleaned with isopropanol, rinsed with deionized water and then dried in nitrogen. Additional crystalline Si (100) substrates were used for complementary characterizations.

Previous work showed that 10-20 mTorr was the optimal pressure range for the fabrication of porous amorphous WO_3 films, achieving EC properties on par with the literature [11], [12]. In the current study, we also explored such films deposited under intense substrate biasing (13.56 MHz RF SEREN power supply) in a large pressure range. The samples were

thus prepared at both 20 mTorr and 1 mTorr with biasing values of up to -525 V; for comparison, a control sample was also produced at 1 mTorr without biasing (floating). Note that lower bias voltages were tested as well; however, as expected, the EC performance decreased with increasing bias up to a threshold voltage of approximately -400 V. Table 4-1 summarizes the main deposition conditions of the samples.

Table 4-1 : Deposition parameters for WO_3 thin films prepared by RF magnetron sputtering.

Sample	Pressure (mTorr)	Substrate bias (V)	Target Power (W)	Target voltage (V)	Layer thickness (nm)	Deposition time (s)	Deposition rate (Å/s)
1	20	0	438	107	136	5500	0.25
2	1	0	438	200	133	875	1.5
3	1	-525	438	201	137	1050	1.3

The deposition rate for samples sputtered at low pressure is vastly increased when compared to the high-pressure samples; in fact, it is more than five times faster in the present context. When biasing is used, the deposition rate is slightly lower; this is attributed to re-sputtering and will be further addressed below.

4.4.2 Film characterization

Cyclic voltammetry (CV) measurements were performed using a PGSTAT302N potentiostat (Methrom Autolab BV) in a three-electrode cell configuration. Tests were made with both H^+ and Li^+ ions. The former ones used a 0.1 M aqueous solution of H_2SO_4 with a graphite counter electrode and a WO_3/ITO sample as the working electrode, while the latter ones used a 1 M $LiClO_4$-propylene carbonate electrolyte with a platinum counter electrode. All tests were performed vs. a saturated calomel electrode (SCE) as reference.

Tests were carried out up to 1000 cycles with an applied potential varying from -0.5 to 1.2 V vs. SCE at a rate of 25 mV/s. An initial bleaching period of 60 seconds at 1.5 V vs. SCE was applied prior to each test. The *in-situ* transmission variation vs. time was obtained with a MultiSpec Pro spectrophotometer (Tec5) equipped with a stabilized white light source and a homemade optical setup. Spectra were acquired in the 350 nm to 900 nm range every 500 ms.

The film thickness and the optical properties were assessed using a RC2 variable angle spectroscopic ellipsometer from J.A. Woollam Co.; measurements were performed at four angles of incidence (45°, 55°, 65°, 75°) from 200 nm to 1700 nm. The properties were derived using general oscillator models to match the layers' optical response in the *CompleteEase* software also from J.A. Woollam Co.

Additional microstructural and chemical analyses were performed using a variety of complementary techniques. Surface topography images (500 nm x 500 nm) were acquired using AFM in the peak force quantitative nanoscale mechanical (QNM) imaging mode using a Dimension ICON instrument from Bruker on samples before and after cyclic voltammetry; the data were then analyzed using the *NanoScope Analysis* software. SEM (JEOL JSM-7600F) imaging at an acceleration voltage of 10 kV of the top surface of the cross-section of the samples was performed to detect structural changes induced by biasing. The crystallinity of the WO_3 was then examined by XRD with a D8 Discover diffractometer from Bruker; these results will not be shown as the films were observed to be XRD amorphous. The films' composition and density were obtained through RBS measurements using a 6 MV Tandem accelerator with a 2 MeV He beam and a 170° retrodiffusion angle.

In order to detect the possible presence of nanocrystallinity, selected area electron diffraction (SAED) patterns as well as high resolution TEM images were acquired with a JEM-2100F transmission electron microscope equipped with a field-emission gun using bright field mode at 200 kV. Samples deposited on silicon substrates were scratched to generate powder and then transferred onto a carbon-coated copper grid while FIB-produced cross-sections were observed on the ITO-samples. The analyzed areas were confirmed to be WO_3 using energy dispersive X-ray spectroscopy (EDX).

4.5 Results and discussion

4.5.1 Optical characterization

Ellipsometric modelling was performed on Si and glass substrates to obtain the optical properties of the WO₃ films and gain insight into their microstructure. All samples were modelled in the bleached state using a combination of a Tauc-Lorentz and Gaussian oscillators for the UV absorption region. Refractive indices at 550 nm were evaluated at 2.06 and 2.24 for the layers prepared without biasing at 20 mTorr and at 1 mTorr, respectively, in accordance with values typically found in the literature for sputtered WO₃ thin films [11], [12]. Modelling of the biased layer (see Table 4-1) required two regions with slightly different optical properties, mainly in the UV. The top layer shows an earlier onset of absorption, suggesting a red-shift of the bandgap in accordance with what is usually observed for heated WO₃ thin films [16]. While this model may be considered as approximate, it is nevertheless an indicator that the film growth is nonuniform and evolves over time. As will be demonstrated below, this in line with the TEM results which indicate the presence of two distinct regions consisting of an amorphous layer overcoated with a nanocrystalline layer. The average refractive index value of 2.18 at 550 nm is thus in between those of the non-biased layers, suggesting a reduced density compared to the non-biased 1 mTorr layer. Although this density reduction and refractive index value can be attained simply by increasing the deposition pressure [12], further characterization shows that biasing grants additional important performance improvements as discussed below.

4.5.2 Electrochemical characterization

Cyclic voltammetry is the preferred method to evaluate the electrochemical activity and stability of EC thin films. Since the coloration/bleaching dynamics are limited by the diffusing ions, protons are often of interest due to their smaller size and thus higher diffusion coefficient. Although this is not a critical factor in the case of smart windows, it is of importance in multiple other applications [11], [12]. Part of the present CV tests are thus run in a 0.1 M sulfuric acid electrolyte where the WO₃ films are consequently exposed to a fairly aggressive environment throughout the duration of the test. Indeed, WO₃ is known to be highly vulnerable to dissolution in water and aqueous acids [17], a phenomenon which

is exacerbated by the addition of a voltage (voltage-enhanced dissolution) [30]. Studies also suggest that the main cause of degradation of proton-based all-solid-state EC devices is chemical degradation of the WO_3 following chemical side reactions [40], [47], [48] and gas formation. Thus, a film capable of withstanding the harsh testing conditions of the present CV tests is expected to perform better in terms of durability when implemented in an all-solid-state device. One may note, that in order to decrease the presence of side reactions, bigger and slower Li^+ ions are often chosen [12]. While this may be beneficial from a side reactions standpoint, other side effects such as charge trapping may also ensue and impact device durability [9].

Additional characterization parameters can be derived from the voltammograms and *in situ* transmission measurements and will be used to supplement the analysis of the electrochemical behaviour. The first and most significant one of these is the coloration efficiency (CE) which quantifies how efficiently a layer colours upon charge insertion; it is expressed as:

$$CE = \ln(T_{bleached}/T_{coloured})/q_{ins} \tag{5}$$

where $T_{bleached}$ is the transmission value at 550 nm in the bleached state, $T_{coloured}$ is the transmission value at 550 nm in the coloured state, and q_{ins} (C/cm^2) is the inserted charge per surface area. Other parameters of interest include the charge extraction ratio, used to quantify charge loss and/or trapping, and the diffusion coefficient, to measure how easily ions travel through the layer [11], [12]. The latter is calculated using the peak anodic current (maximum current during the bleaching phase).

Preliminary experiments showed that all samples deposited at low pressures with bias voltages lower than -400 V exhibited the expected poor EC performance, with colour shifts of approximately 20% at best (see Figure 4.1) and an even worse performance for higher bias values. However, above a threshold potential, the electrochromic activity of the material was seen to suddenly greatly increase. It is also important to note that samples

deposited at higher pressures (20 mTorr) were negatively impacted under all bias values (not shown here).
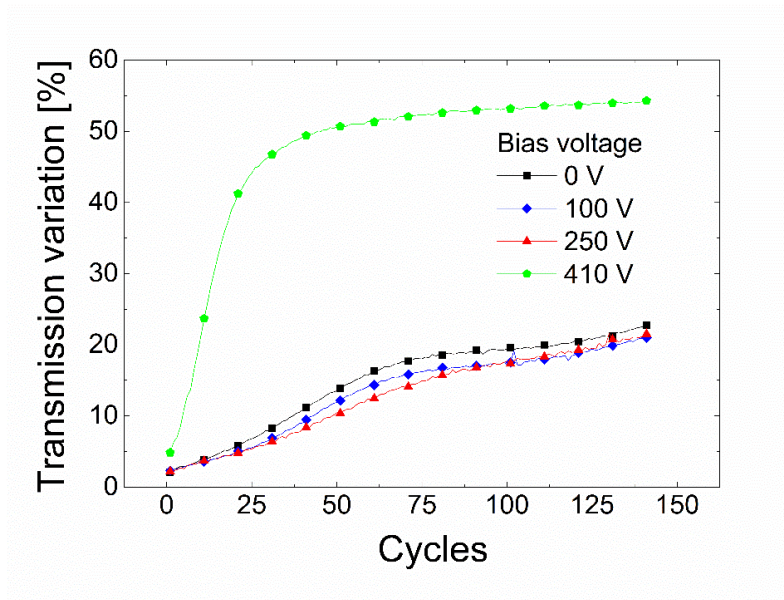
Figure 4.1: Transmission variation (ΔT) of preliminary samples of WO_3 prepared with various applied substrate biases.

Further experimentation revealed that samples prepared at -526 V of bias (highest attainable bias on the deposition system under the present conditions) offered the best performance. The main results of the proton insertion tests for such a sample are presented in Table 4-2.

The cyclic voltammograms for the first 150 cycles with proton insertion and corresponding optical measurements are shown in Figure 2. As expected, the traditional porous film prepared at 20 mTorr (2.67 Pa) displays a very intense initial EC activity, but shows a steady degradation over time. The variation of the bleached state transmission is attributed mostly to changes in the optical thickness through voltage-enhanced dissolution [12] of the layer; this decrease in thickness results in a shift of the interference fringes and thus the oscillating nature of the transmission curve in Figure 4.1 and the initial increase in transmission over 100%. These side reactions can also explain the 90% charge extraction ratio as charge trapping is expected to be low in such a porous film; indeed, a 99% charge extraction ratio is found when using bigger Li^+ ions (not shown here).

Table 4-2: Electrochromic parameters for proton insertion (initial-final values after 150 cycles). Average values are used instead when the variation throughout the test is judged as negligible.

Sample	Coloration efficiency (cm^2/C)	Diffusion coefficient ($10^{-10}\ cm^2/s$)	Charge extraction ratio (%)	Transmission variation @ 550 nm (%)
1 - High pressure	65-35	220-60	90-85	53-20
2 - Low pressure	60	0.1-12	45-70	3-22
3 - Biased	69	60-120	90	50
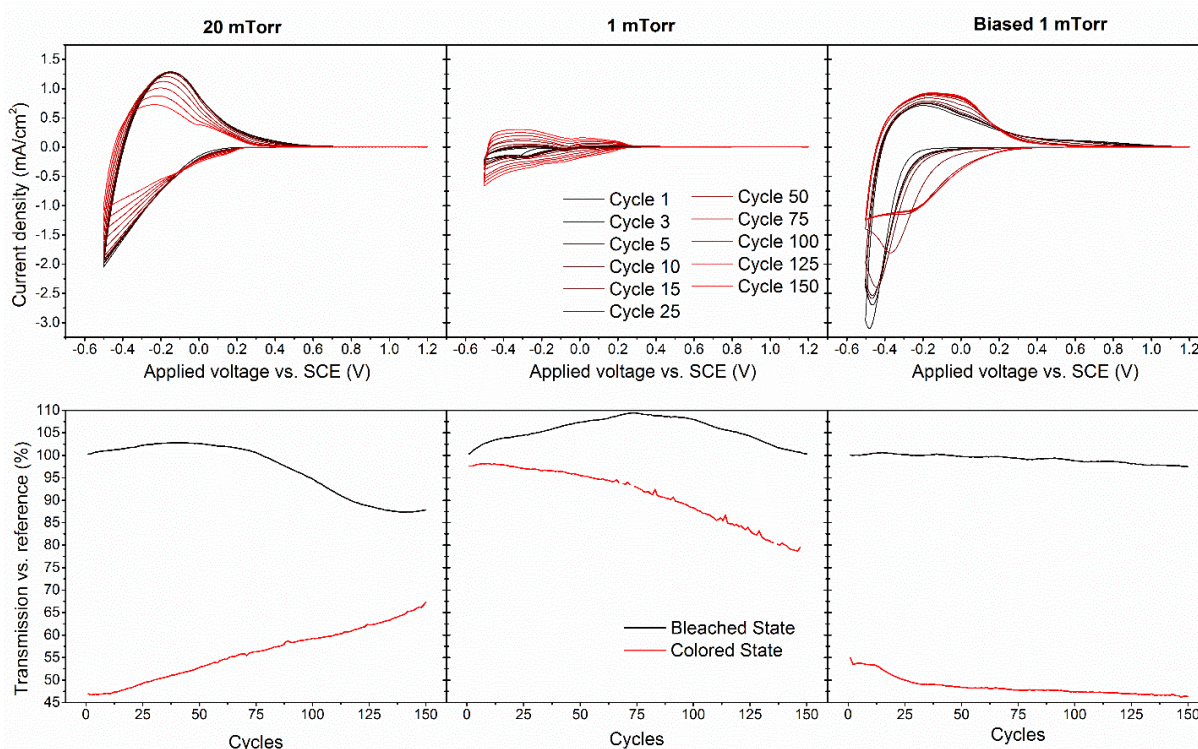
Figure 4.2: Cyclic voltammetry tests at 25 mV/s in 0.1 M H_2SO_4 over 150 cycles (top) for the 20 mTorr-deposited WO_3 layer (left), 1 mTorr-deposited layer (middle) and biased 1mTorr-deposited layer(right) with transmission in the maximum bleached and coloured states at 550 nm (bottom). Note that the reference 100% transmission was performed in the samples' bleached state and as a result, the absolute transmission variation is 10-20% lower.

The coloured state also exhibits a continuous increase over time, indicating a decrease in charge insertion as observed on the voltammograms due to (once again) film dissolution in the electrolyte. Overall, the film shows an initially good performance, but its quick degradation in an acid electrolyte is not surprising. This decay is also reflected in the change in coloration efficiency from 65 to 35 cm^2/C, as well as the reduction in diffusion coefficient from 22 x 10^{-9} cm^2/s to 6 x 10^{-9} cm^2/s, and the significant loss in ΔT from 53% to 20% (see Table 4-2).

The measurements for the low-pressure sample (1 mTorr) deposited without biasing show a poor EC performance, with a diffusion coefficient two orders of magnitude lower than in the previous case at the beginning of the test (lower than 0.01 x 10^{-9} cm^2/s and peaking at 1.20 x 10^{-9} cm^2/s). There is, however, a considerable increase in coloration at higher cycles which can be attributed to the creation of channels within the layer through continuous insertion/extraction of ions, resulting in a facilitated ion intercalation (activation period); the variation in transmission nevertheless remains low, with a maximum value of 20 %. The bleached state transmission shows a variation similar to what was observed with the 20 mTorr sample but at a lower level as the dissolution speed is decreased. The voltammograms also exhibit an unusual shape with secondary peaks appearing at -0.05 and -0.3 V, which have been attributed to sub-steps in the tungsten reduction process, from W^{6+} to W^{5+} and W^{5+} to W^{4+}, respectively [25]. This two-step ion insertion process is thought to be more visible in this unbiased sample because of the greatly reduced intensity of the peaks compared to the porous sample (the currents are ~10 times lower.) At higher currents, theses peaks are seen to convolute as the number of available diffusion pathways with different energy requirements increases thus broadening the peaks and leading to more continuous-looking voltammograms, as can be seen for later cycles. These peaks are also known to be a sign of the possible presence of crystallinity in the films as will be addressed in section 3.3. The measurements confirm that the unbiased low pressure WO_3 film is quite poor electrochemically, and although denser it still suffers from dissolution; this is also confirmed from the visual inspection of the sample which appears diffusive to the naked eye following 150 CV cycles.

The layer deposited with biasing offers the best characteristics thus far with a CE of 69 cm^2/C, a diffusion coefficient varying from 6 x 10^{-9} cm^2/s to 12 x 10^{-9} cm^2/s from start to finish, and a stable 90% charge extraction ratio, as well as a short activation period. These parameters are similar to those of the traditional porous sample in terms of coloration dynamics. Additionally, the ΔT is stable at 50 % for most of the duration of the test, after a sharp increase at the beginning attributed to the same channel creation mechanism observed in the previous dense sample. Contrary to the porous film, the chemical stability of the biased film exhibits negligible variation over 150 cycles; this can be deduced from the stable and even increased surface area of the voltammograms as well as the stable ΔT (see Figure 2). The slow drop in the bleached state transmission (3% over 150 cycles) is most probably related to some amount of deep charge trapping as discussed by Wen *et al* [9] and the result of the 90% charge extraction ratio. Indeed, contrary to other samples, no change in appearance of the layer is visible to the naked eye, suggesting a negligible amount of layer degradation. We can also observe in the voltammograms that the peak at -0.3 V, which has been associated with the presence of W^{4+}, is more prominent than in the non-biased samples. This peak has also been linked to the coloration of WO_3 in nanocrystalline samples [25], and it thus suggests its possible presence in our biased samples. Raman measurements of the samples (see supplementary data) also point towards crystallinity, with two peaks around 800 and 700 cm^{-1} for the biased sample, and a single broader peak for the other samples. A similar effect has been observed by Shigesato *et al.* [49], where crystalline WO_3 exhibited two peaks at 719 and 807 cm^{-1}, while a-WO_3 only displayed a broad peak associated with the W-O stretching bond. The rather broad nature of the two peaks in our case may indicate that the sample is only partially crystalline.

The performance enhancement following biasing may seem counterintuitive. Indeed, biasing is known to normally increase the density of layers by providing additional kinetic energy to the sputtered atoms. However, studies have shown that for higher bias values, the energy increase can have adverse effects on the morphology [40], [50]. Specifically, above a certain threshold voltage, which depends on the mass ratio of the gases and material being sputtered, the layer growth enters a regime where re-sputtering of the layer is non-negligible, and other phenomena such as argon trapping, preferential sputtering of oxygen,

and defects creation (missing or misplaced atoms) can occur [17], [37], [42]. We thus believe that, in the present case, such structural changes are beneficial for the EC performance of WO_3 films by increasing their porosity and thus allowing for the facile insertion of ions into the layer. Micropores caused by re-sputtering have been identified before [50]. The increased stability could then be linked to the crystalline nature of part of the constituent film. All of these considerations are addressed in section 3.3.

Finally, an extended CV test was performed under the same conditions as the previous ones for 1000 cycles, with a total duration of 40 hours, in order to better evaluate the long-term durability of the biased sample. The obtained CV curves and transmission variation are shown in Figure 4.3. The CV curves are seen to stabilize after the first 300 cycles while continuing to slightly increase in current both during insertion and extraction. There is also an important bleached state transmission reduction over the course of the test ($\Delta T = 25\%$), which is attributed mostly to ion trapping (90% charge extraction ratio). This results in a ΔT variation from 50% initially to ~35 % at the end of the test. Although this is a significant reduction, it is still much better than what was observed after only 150 cycles for the 20 mTorr sample. We can therefore conclude that the 1 mTorr biased sample shows an excellent EC performance and an exceptional chemical durability when compared to the 20 mTorr WO_3 layer described above, offering great potential for long-term proton insertion applications. In addition, we believe that further optimization of the pressure and bias voltage can further enhance the performance; preliminary results (not shown here) indicate that this is indeed the case.
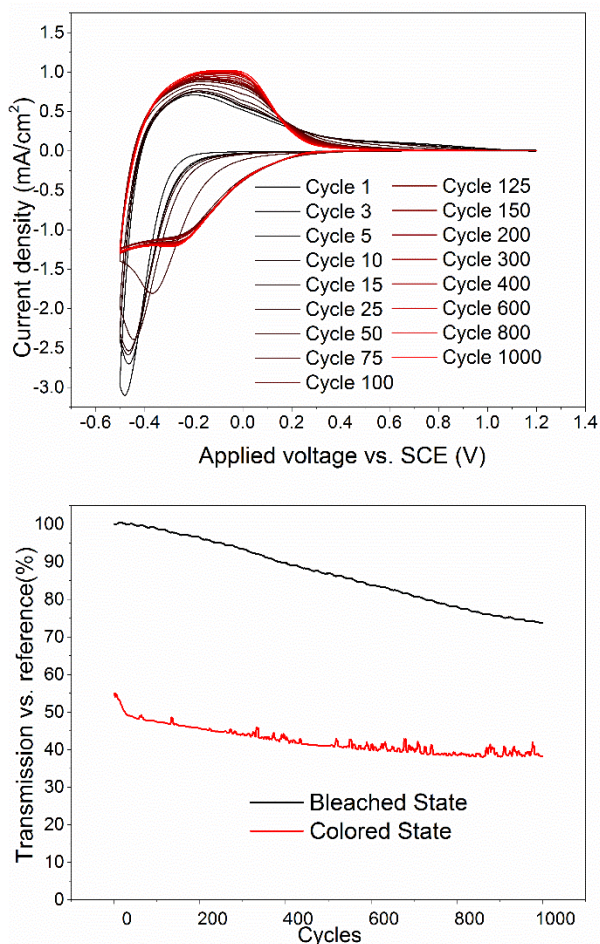
Figure 4.3: Proton-based cyclic voltammetry test over 1000 cycles for the biased 1 mTorr WO₃ layer (top) and transmission in the maximum bleached and coloured states at 550 nm (bottom). Note that the reference 100% transmission was taken in the bleached state.

Lithium insertion being the favoured method of colouring WO₃ layers due to an increased chemical stability, all the samples were also tested with a lithium-based electrolyte. Although not shown here, the performance of the biased layer was slightly poorer than in the case of protons (rapid drop in the bleached state transmission of 5% in the first 10 cycles before stabilizing into a similar behaviour). This reduced performance is attributed to the larger size of the Li^+ ions which clearly have more difficulty diffusing through the layer. Further optimization would most probably remedy this issue and will be the object of further studies.

4.5.3 Structural and morphological characterizations

Following the CV tests, structural and morphological characterizations of the samples were performed to better understand the effect of biasing and its ability to enhance the EC performance of samples sputtered at low pressures. It is known that the microstructure plays an essential role in the charge injection process which colors WO_3 and that it is along the network of voids in the material where ionic transport occurs [42]. Therefore, an increase in the amount of interconnected voids in the film should result in an increased EC performance.

To begin with, the surface of the samples was analysed by AFM. This allowed us to observe both the impact of biasing as well as of CV degradation on the morphology of the layers. Figure 4.4a shows the surfaces of the three reference samples before CV testing.
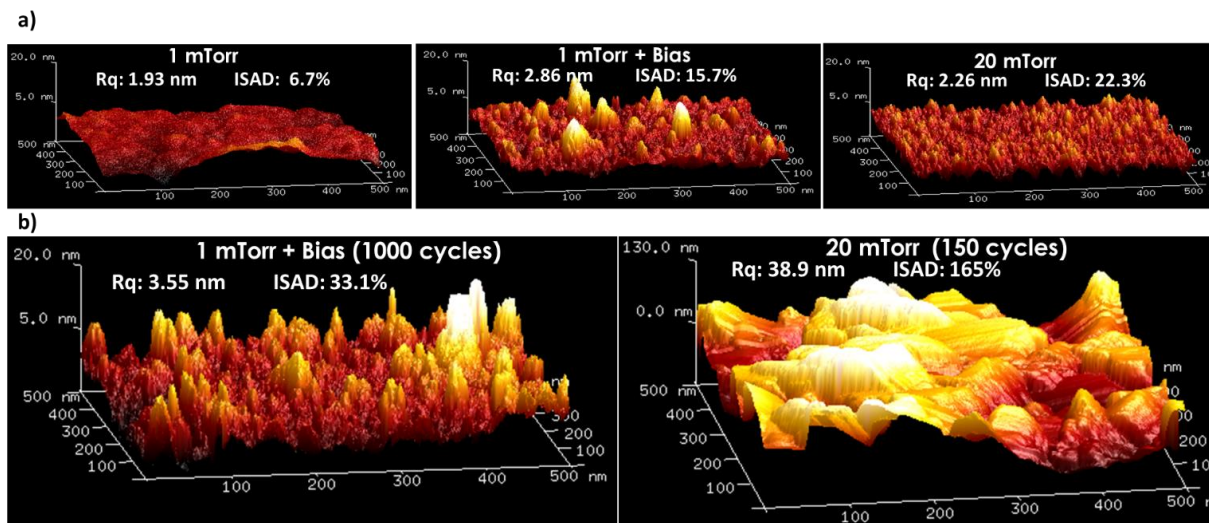
Figure 4.4: AFM measurements of a 500 nm x 500 nm surface for a) as-deposited samples before CV tests (top) and b) after CV tests (bottom). The RMS roughness (Rq) and integrated surface area difference (ISAD) are also displayed on the images.

It is clear from these images that biasing results in an increased surface roughness in comparison to the 1 mTorr non-biased layer and a less homogeneous surface with larger localized peaks. The RMS roughness value, Rq, is in fact slightly higher than the 20 mTorr film as well (2.86 nm vs. 2.26 nm). Another interesting metric is the integrated surface area

difference (ISAD), which represents the area difference between the surface and its projection. This value is significant because it reflects the available surface area for ion insertion, which is a critical parameter for the electrochromic dynamics at the electrolyte/surface of the film interface. We can see that although the bias-assisted process results in more intense localized peaks, the high pressure sample nevertheless displays a higher uniformity and a larger surface area. In addition, the re-sputtering porous microstructure-inducing process is in fact present during the whole growth process so that we may assume that defects such as pores and interconnected channels are also present in the bulk of the film.

To confirm the film's durability towards chemical degradation, measurements were also performed on the layers after cycling for the bias-deposited and 20 mTorr layers (see Figure 4.4b). The biased layer shows an increase of Rq and ISAD after the 1000 cycles of CV testing, indicating that it has been somewhat degraded. However, the damage remains limited as the morphology is quite similar. Ellipsometric measurements also suggest a limited decrease in thickness (< 5 nm) and an increase in roughness (from 5 to 10 nm). In contrast, the 20 mTorr layer shows a very intense degradation after already 150 cycles, with complete parts of the film having seemingly been removed. In fact, not only is the roughness higher, the maximum variations are much larger with the highest peaks having a height of 130 nm; in other words, a value equal to the thickness of the layer and thus confirming that the layer has been completely removed in some areas. These measurements clearly indicate increased durability of the biased sample compared to the 20 mTorr layer which exhibits the devastating effect of an aggressive H_2SO_4 environment.

Following the AFM surface analysis, we now investigate the bulk of the layer. SEM images of biased and non-biased samples of WO_3 layers prepared at 1 mTorr on Si substrates allow us to better understand the effect of biasing on the microstructure of the films. The images were taken at a slight angle in order to observe both the cross-section and the surface of the samples at the same time (see Figure 4.5).
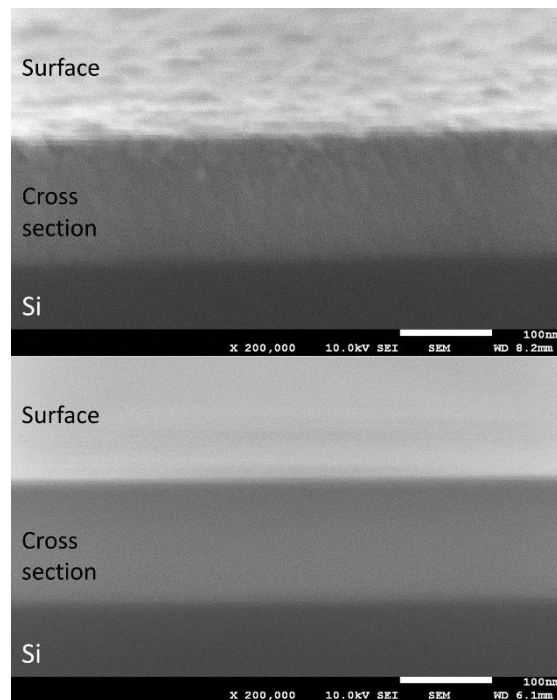
Figure 4.5: SEM images of WO$_3$ samples prepared at 1 mTorr: the biased sample is shown on top and the non-biased on the bottom.

It can be clearly observed that biasing affects the microstructure of the layer. The 1 mTorr sample is smooth and featureless, while the biased sample has a columnar-like microstructure with a very rugged surface. This is in agreement with the structure zone model, where biasing of a few hundred volts in magnitude allows either a zone *T* type of growth, characterized by "densely packed fibrous grains", or zone 3 growth, defined as "fine-grained and nanocrystalline" for these energies [37]. The result for our films seems to be a pseudo-porous structure, causing an impressive gain in EC performance through higher surface area and easier ion intercalation.

To better evaluate the porosity, density and chemical composition of our WO$_3$ films, RBS measurements were also performed on all the samples. The obtained values are presented in Table 4-3.

Table 4-3: Atomic composition of the WO_3 samples determined by RBS measurements.

Sample	W (%)	O (%)	O/W ratio	Ar (%)
20 mTorr	22.2	77.7	3.5	0.0
1 mTorr (unbiased)	25.0	73.0	2.9	1.8
1 mTorr (biased)	23.8	73.2	3.1	2.8

The presence of argon in the low-pressure samples, and in higher concentration for the biased one, is worth mentioning. This indicates that there is some argon trapping occurring during deposition and that it is accentuated by biasing. The analysis also reveals that the 1 mTorr layers are very close to the WO_3 stoichiometry with a O/W ratio of 2.9 for the unbiased and 3.1 for the biased sample, with the biased sample being slightly over-stoichiometric, while the 20 mTorr layer shows a 3.5 O/W ratio. Both higher-than-3 ratios could however be explained by the presence of chemically absorbed water in the layer, even more so in the case of the very porous 20 mTorr sample. This would indicate that the biased sample in its as-prepared state absorbs more water than the unbiased one, but less than the high-pressure layer once again in agreement with the density measurements.

Knowing the surface atomic density of the layers and their thickness through ellipsometry allows us to approximate the density and packing density (calculated using a bulk density of 7.16 g/cm^3 [16]) of the samples. Through the use of an effective medium approximation, specifically the Lorentz-Lorenz model, we can also calculate the packing density of the layers [12] using the refractive index to compare with the RBS results. These values can be found in Table 4-4.

Table 4-4: Density and porosity of the WO₃ samples through RBS and ellipsometry measurements.

Sample	Thickness (nm)	Density (g/cm³)	Packing density by RBS (%)	n @ 550 nm	Packing density (Lorenz-Lorentz) (%)
20 mTorr	136	5.2	72.6	2.06	81.6
1 mTorr (non-biased)	133	6.5	90.8	2.24	90.0
1 mTorr (biased)	137	6.1	85.2	2.17	86.9

We can immediately see that the low-pressure sample is denser than the high pressure one, in accordance with our expectations. These results confirm that the biased layer is at an intermediate state between the porous 20 mTorr and the dense 1 mTorr layer. Also, while considering the packing densities obtained by RBS and using the Lorentz-Lorenz effective medium approximation (EMA) match for the two 1 mTorr samples, the 20 mTorr sample shows a higher value in packing density obtained from the EMA calculation. This difference can be explained by the limitations of the model which assumes homogeneously dispersed nano-sized inclusions throughout the layer [51]. This discrepancy between the results could thus be attributed to the inhomogeneous nature of the film or to its higher water content which is not considered in the model; note that a Bruggeman EMA was also tested and did not work well for all samples.

Finally, although all films were observed to be XRD amorphous, TEM measurements of the samples were performed to confirm the possible presence of bias-induced nanocrystallinity as observed, for example, by Madhavi *et al.* [40]. The imaging was first made on WO₃ particles which were scratched-off the Si samples using a diamond tip; the analyzed sections of the collected material were confirmed to be pure WO₃ through EDS measurements. The analysis of the non-biased sample confirms that it was indeed

amorphous. Correspondingly, the SAED image shows diffuse concentric rings, characteristic of an amorphous material (see Figure 4.6).
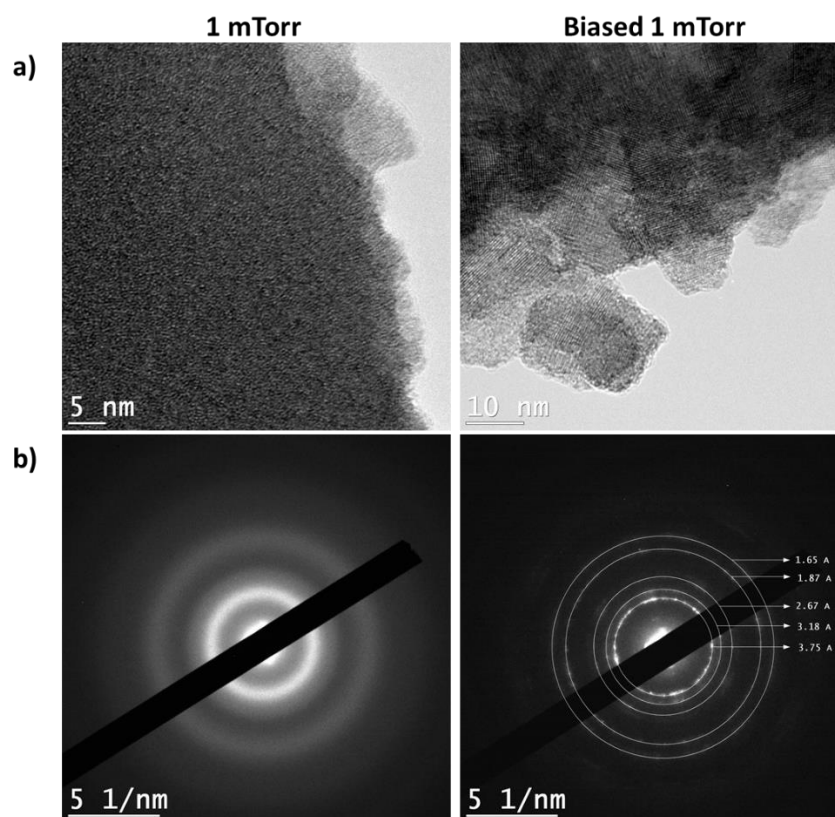

Figure 4.6: a) TEM powder imaging (top) of the 1 mTorr WO_3 (left) and biased 1 mTorr WO_3 (right) with b) corresponding SAED image (bottom).

Measurements performed on the biased sample revealed much more interesting results. Although parts of the collected particles were amorphous, a presence of nanocrystallinity was observed. This can be clearly seen in Figure 4.10 where crystalline grains around 10 nm in size are present, but may be too few to be detected by XRD. These grains display clearly defined concentric rings on the SAED image, confirming the polycrystalline nature of the analysed material. Additionally, the interplanar spacing obtained from the SAED data, yields a value closely matching the monoclinic WO_3 crystal system [JCPDS no. 431025]. It is clear from these two measurements that the use of significant substrate biasing promotes nanocrystallinity in WO_3.

This bias-induced crystallization was further investigated with TEM imaging on samples deposited on ITO and properly prepared by focused ion beam. Figure 7 shows the results for the non-biased and biased samples, respectively. The first image on the left shows the smooth and amorphous microstructure expected for the low-pressure-deposited WO_3. The image on the right is, however, much more interesting as it appears that the biased layer initially starts in an amorphous state and then undergoes a transition into a polycrystalline state partway through the deposition. The transition from amorphous to crystalline is most probably the result of the increase of the sample's temperature as a function of time due to the process itself and at which point the additional surface energy supplied by the incoming ions allows for the film to reach a critical onset of crystallization (~350°C for WO_3). It is, at present, unclear which of these regions is responsible for the observed increased durability and performance over the non-biased WO_3 films, although we suspect that both probably play a role. A similar combination of a protective, denser top layer covering but not inhibiting a porous, more fragile WO_3 layer has indeed been studied by Azens et al. [52].

The morphology of the layer also has a significant impact on its performance as a larger internal volume is essential for proper ion intercalation. Studies have shown that annealing gives control over the size of the nanocrystals, in order to optimize for the best EC performance [36], [53], [54]. These same studies have found optimal temperatures around 200°C, past which the crystal sizes grew too large to allow for adequate EC properties. This suggests that a similar crystallite size control could be obtained using the present process by modifying the deposition parameters in order to reach an optimum crystal size and morphology, especially if the crystalline transition is indeed caused by heating through ion bombardment. The presence of trapped argon in the films may also allow for the creation of pre-existing air pockets and thus pathways for ionic diffusion. The intense ion bombardment also visibly causes defects, "deteriorates" the films' surface uniformity and creates more space in the lattice - all, a priori, beneficial from a diffusion standpoint.
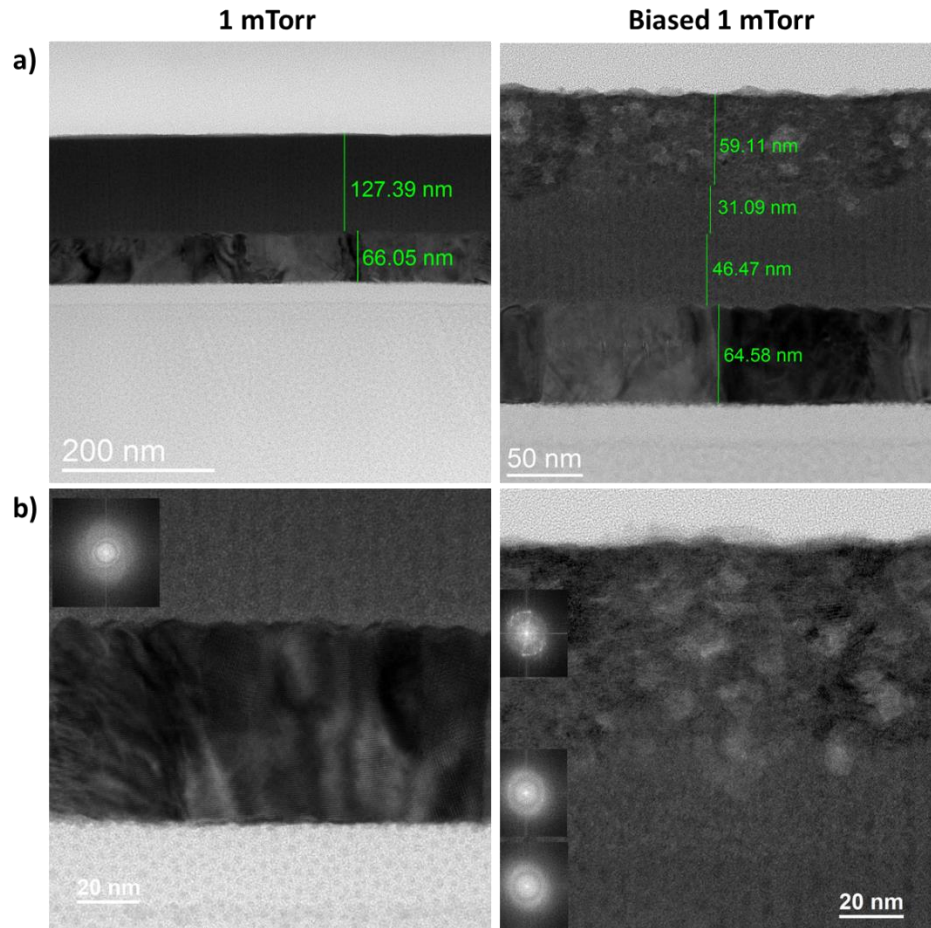
Figure 4.7: a) TEM imaging of a 1 mTorr WO_3 layer (left) and a biased 1 mTorr WO_3 layer (right) on ITO-covered substrates with indicated thicknesses in green (top) and b) SAED information for the WO_3 thin films (bottom).

Finally, the presence of nanocrystallinity is not only important from the durability point of view, but also from the energy perspective as polycrystalline WO_3 films have been shown to display a more Drude-like behaviour and thus reflection-based modulation as a function of intercalation [16]. The transfer from absorption to reflection-based modulation is of obvious importance for architectural applications as this will limit the amount of absorbed solar energy and consequently black body infrared re-emission.

4.6 Conclusions

A novel fabrication approach for electrochromic WO_3 thin films using high substrate biasing to enhance its EC activity has been demonstrated. When compared to previous best performing layers deposited at higher pressures, those prepared at low pressure and high bias voltage (over -400 V) demonstrate vastly increased durability, similar EC activity, and five times higher deposition rates. The ability of substrate biasing above a critical threshold to enhance WO_3's EC performance is attributed to the creation of a pseudo-porous nanostructure (void network) possibly through argon bubbles and defects, as well as the presence of nanocrystallinity. This hypothesis is supported by SEM imaging which shows a change in microstructure, RBS and ellipsometric measurements showing an increase in porosity, and AFM surface analysis detecting higher peak roughness after biasing, as well as TEM imaging showing clear polycrystallinity at the nanoscale in the biased samples. Cyclic ion insertion is thought to open channels to pores present throughout the layer (activation period), allowing for easier subsequent insertion and thus increasing the performance over time.

As a limited amount of optimization has been performed, especially concerning the use of lithium ions, we believe that there is still much room for improvement, particularly by exploring heating during or after deposition, and fine-tuning the pressure and applied substrate bias as the WO_3's EC properties are directly linked to its morphology. Finally, as nanocrystalline WO_3 is highly coveted for EC devices, especially mesoporous structures [32], our approach has the benefit of not requiring any chemical preparation steps or post deposition annealing to obtain the desired nanocrystallinity as well as allowing for much faster deposition rates than in the context of the deposition of traditional porous a-WO_3 by magnetron sputtering. Further experimentation will focus on obtaining only the amorphous or the crystalline phase of the biased WO_3 layer by controlling the heating of the sample and deposition time in order to separately evaluate their properties. Modelling the growth of WO_3 under high energy bombardment conditions is also expected to bring further understanding of the microstructural evolutions.

4.7 Acknowledgements

CHAPTER 5   GENERAL DISCUSSION AND PERSPECTIVES

5.1 Nanocrystalline WO₃

5.1.1 Results

WO_3 electrochromic thin films were deposited using RF magnetron sputtering with the addition of substrate biasing to modify their microstructure. By reaching a bias voltage of -525 V the properties of layers prepared at a low pressure of 1 mTorr were significantly modified through intense ion bombardment. It is interesting to note that a threshold value must exist for the appearance of these effects and has been observed to be as low as -410 V on a smaller deposition system.

The refractive index at 550 nm reached 2.17, a value in between a non-biased 1 mTorr WO_3 at 2.24 and a more porous 20 mTorr WO_3 at 2.06. Using the Lorentz-Lorenz EMA, a packing density value of 86.9 % was found for biased layers, compared to 90.0 % and 81.6 % for the low- and high-pressure samples deposited without biasing respectively, closely matching the values calculated from the RBS results of 85.2 %, 90.8 % and 72.6 % obtained for the same films. The discrepancy for the more porous sample can be attributed to the inhomogeneous nature of the film or to absorbed water not considered by the model. A decrease inthe deposition rate from 1.5 to 1.3 Å/s was also observed when biasing was implemented at 1 mTorr and mainly attributed to the presence of re-sputtering. However, this value remains much higher than the 0.25 Å/s rate at 20 mTorr. Composition analysis with RBS also reveal an higher quantity of argon in biased films (2.8 % vs 1.8 %) for the low-pressure samples and none at 20 mTorr, suggesting that there could be microbubbles of trapped argon in the denser films. In summary, these results indicate an increase in porosity when substrate biasing at high enough energies is added to the deposition, attributed to re-sputtering, argon trapping and creation of defects, such as missing or displaced atoms perturbing the structure.

AFM and SEM imaging allowed us to observe a significant increase in surface roughness for the biased samples which, by increasing the total accessible area for the electrolyte, can be beneficial from ion insertion point of view, especially if the electrolyte is in liquid form. Raman spectroscopy indicated the presence of nanocrystallinity in the biased samples, an effect that was later verified by the observation of nanocrystalline grains using TEM imaging. The latter also revealed two

distinct regions in our films, indicating that the growth of the film transitions from amorphous to nanocrystalline approximately partway through the deposition process. This change is attributed to an increase in the system's total energy dissipated during the deposition, meaning an increase in temperature which with the addition of the ion bombardment leads to the onset of crystallization. The induced collisions can be the source of thermal spikes, the deposition of a high density of energy in a localized area [34]. This could mean multiple small regions starting to crystallize after an impact, in line with the observation of small grains (50 nm or less) in the polycrystalline structure of the films.

The presence of a nanocrystalline layer on top of an amorphous one can possibly serve as a key feature allowing for identification of thin films prepared using this method in the context of the patent filed with our partners (Guardian Industries and Essilor) for the method, and one of the reasons for observing such a high durability. Indeed, crystallization of WO_3 layers usually requires heating which typically leads to the crystallization of the whole film. Ellipsometric modelling also agreed with the presence of two distinct regions with slightly different optical properties.

Along with structural and optical characterization, electrochemical cyclic voltammetry tests revealed an increased EC performance for biased films. Values of coloration efficiency of 69 cm^2/C were achieved that are comparable to the 65 cm^2/C of regular porous layers, as well as diffusion coefficients of 120 x 10^{-10} vs 220 x 10^{-10} cm^2/s), charge extraction ratios of 90 % for both films and transmission variation of 50 % vs 53 % before degradation. The main difference between the films is their cycling durability; while the 20 mTorr WO_3 saw intense degradation of its transmission variation over the course of 150 cycles (a drop from 50 to 20%), the biased layer showed little to no change. These changes were confirmed by AFM imaging of the samples after cycling. An extended test of 1000 cycles on a biased film demonstrated a loss of ~25 % of ΔT, still less than the loss of the 20 mTorr sample after only 150 cycles. Additionally, while the high-pressure sample had variations in both its maximum and minimum transmission, indicating a loss of material, the biased sample had a stable minimal transmission, suggesting that ion trapping is responsible for the diminishing performance. This is a problem that could potentially be resolved by applying a high positive voltage to de-trap some of the ions, a method called rejuvenation as coined by the group of C.G. Granqvist [9]. The same electrochemical tests have been done using an electrolyte composed of lithium perchlorate in a polycarbonate solvent for Li^+ ion insertion. This alternative

cation is usually favored for its lower tendency to chemically degrade films. It is however much larger than hydrogen and for our biased films this resulted in heavier trapping. The explanation is probably that the diffusion channels are smaller in the biased film. Even with hydrogen, the initial coloration is low and an activation period is observed, during which ion channeling is expected to open access to some of the pores in the material. The material might simply be too dense, especially the crystalline top layer, for this to occur with the lithium ions.

Surprisingly, the films that were produced in a deposition system with a smaller chamber showed no signs of degradation after 1000 cycles. The reason for this is not clear but one of the main differences between the systems is the distance between the magnetron and substrate holder. This could result in ions arriving with more energy if less collisions occur and an earlier transition into the crystalline state. The chamber also tends to heat because of the energy dissipated from the plasma, which could favor crystallisation. The flux of ions must also be higher, which will also have an important impact on the growth of the film. Overall, the resulting film sshould be denser or have a thicker crystalline top layer, which would explain the increased durability. The film also has a much slower activation period (around 50 cycles), meaning that the ions have a harder time channeling through this denser or thicker protective layer. These results do tell us that by further optimizing the deposition process, the performance of biased films can also be further improved to strike a balance between EC activity and durability.

5.1.2 Outlook

The present study clearly underlined that significant substrate biasing leads to an enhanced EC performance, however, at this point, it is difficult to conclude if these phenomena can be attributed solely to a more resilient amorphous underlayer, to a more robust crystalline top layer or to a combination of both. A likely possibility is that the crystalline layer serves as a barrier protecting the amorphous layer from chemical attack and side reactions at the surface, while still allowing sufficient ionic diffusion. In that case, while most of the coloration would come from the underlying layer, the top layer could still be partly active. This concept for increasing device performance is actually quite similar to what was previously investigated at the FCSEL where an overlaying dense layer did not inhibit the coloration of underlying porous film [12].

In order to gain more insight into the phenomena related to the microstructure-EC property relationship, additional investigations should be considered. Since the increase in the total deposition energy is thought to be responsible for the transition from amorphous to crystalline growth, temperature control during deposition could allow one to isolate these effects. Stopping the deposition right before the transition occurs for a cooling period could allow for the growth of a totally amorphous layer. Inversely, different temperature setpoints could be investigated to see if it is possible to trigger an earlier crystalline growth without going above the 350 ºC temperature known to fully crystallize WO_3. These layers could then be investigated individually to observe their respective performance. If the hypothesis that the top layer acts as a shield is confirmed, controlling the process to obtain more amorphous material and a thinner top barrier to protect it could result in increased coloration and higher durability, e.g.: by only applying the bias voltage towards the end of the deposition process. While important information could be gained from realizing such a series of samples, confirming their amorphous or crystalline nature would require, as previously shown, TEM imaging.

It seems clear at this point that the key to obtain this enhanced EC performance is to prepare a nanocrystalline WO_3 layer structured in a way that increased porosity is obtained without traditional heat-treated (annealed) c-WO_3. As indicated in Chapter 2, other methods such as sol-gel, can be used to do so, but substrate biasing appears a much simpler and possibly more cost-effective (from an industrial point of view) approach. However, as mentioned in that same chapter, biasing only provides control of the energy of ion bombardment, which is only half of the equation. Using an ion beam instead would allow one to also selectively control the ion flux. Precisely adjusting both parameters might in turn lead to new changes in the microstructure. Depositing WO_3 in a system equipped with an ion gun is an interesting avenue to further pursue this project.

We discovered an unexpected yet very interesting effect in the context of the electrochromic properties of WO_3 films which only manifested itself at very high energies. In the available literature on the subject, most of the research was performed for bias potentials lower than -200 V and in the case where higher voltages are implemented, the authors often observe interesting phenomena which are judged as detrimental for their application and thus not clearly explained nor investigated. The present research shows that in some cases, it might be worthwhile to pursue this investigation, if the material could potentially benefit from nanocrystallization or the deposition of

dense films with structural porosity for example. For instance, the GLAD WO_3 films prepared by another member of the FCSEL, Julien Gagnon, were shown to have enhanced properties when ion bombardment was implemented. The deposition of NiO films, which require many of the same structural properties as WO_3 when used as an ion reservoir and complementary electrochromic layer, is another interesting candidate for high energy ionic bombardment assisted deposition.

5.2 Electrochromic Security Devices

The biased material's enhanced performance is important not only in the context of smart windows but also other applications, such as security devices. In parallel with my research on the bias-assisted deposition process, I also worked on developing small sized (1-3 cm^2) electrochromic optically variable devices instead of smart windows. The FCSEL has a history of working on such devices in the past (see Bill Baloukas' work [15]) and had an ongoing Idea to Innovation (I2I) grant from NSERC for a project with Nanotech Security Corp. on the subject. Counterfeiting causes significant issues worldwide and as passive angular color shifting metal-dielectric filters are becoming easier to copy, new features with a higher technological complexity are needed to stay ahead of counterfeiters. Combining the passive Fabry-Perot-like optical filter (Metal / Dielectric / Absorber) with an active WO_3 layer results in a 2-level authentication device of potential interest for the next generation of security features. Since security devices often require long-term usage, a more durable WO_3 would be of obvious interest. There are however, other limiting factors which needed to be improved upon.

We decided on an all-thin-film (ATF) electrochromic device for several reasons. First, having an oxide-based electrolyte should result in less side-reactions and therefore chemical degradation than a polymer-electrolyte-based design. Second, an ATF device can be deposited all at once without breaking vacuum for a "cleaner" process resulting in devices less prone to short-circuiting. Third, and most importantly, the goal being to combine interference and active effects, the total optical thickness needs to be maintained low enough to interact with visible light, which is not possible with thicker polymer electrolytes.

 A regular electrochromic device is composed of two electrodes, an ion reservoir, an electrolyte and the electrochromic layer. Usually, in a transparent configuration, both electrodes are transparent conductive oxides (ITO for example) and nickel oxide and tantalum oxide serve as good ion reservoir and electrolyte respectively (see Figure 5.1).
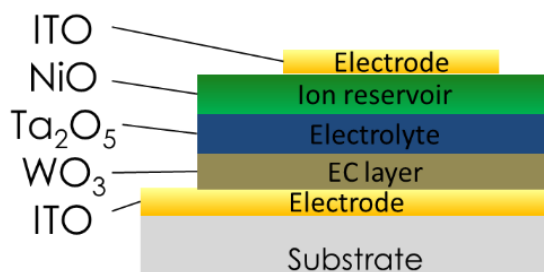

Figure 5.1: ATF electrochromic device.

This design happens to be very close to the classical design of a Fabry-Perot-like metal-dielectric filters (see Figure 5.2)., where a cavity is formed between two reflective layers and by controlling the thickness of this cavity (dielectric spacer) one can control the resulting color. By changing the viewing angle, the optical thickness varies and so does the color. Making the top layer out of very thin chromium film (5 to 8 nm) has been shown to result in a highly saturated color [55].
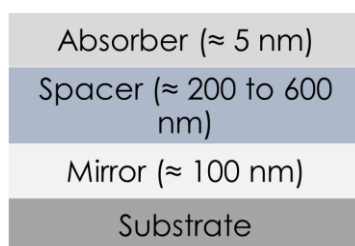

Figure 5.2: Fabry-Perot-like metal-dielectric filter.

The ion reservoir, electrolyte and electrochromic layers of the ATF EC device can be viewed altogether as the dielectric spacer. We can then simply replace one of the ITO electrodes with aluminum to serve both as a mirror and an electrode and add the absorber at the other end. We kept the other ITO layer because the Cr layer was too thin to function as a good conductor and for simplifying the deposition process (no additional masking is required to access the Cr film) and obtain the design presented in Figure 5.3.
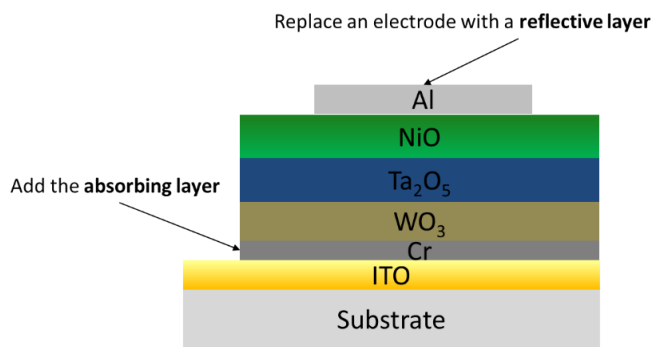

Figure 5.3: ATF electrochromic device combined with Fabry-Perot-like filter design.

By choosing appropriate thicknesses for the dielectric layer, a clear change in color between the bleached and colored states, as well as a significant angular color-shift can be achieved (see Figures 5.4 and 5.5)
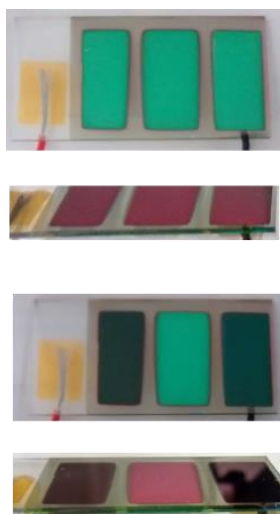

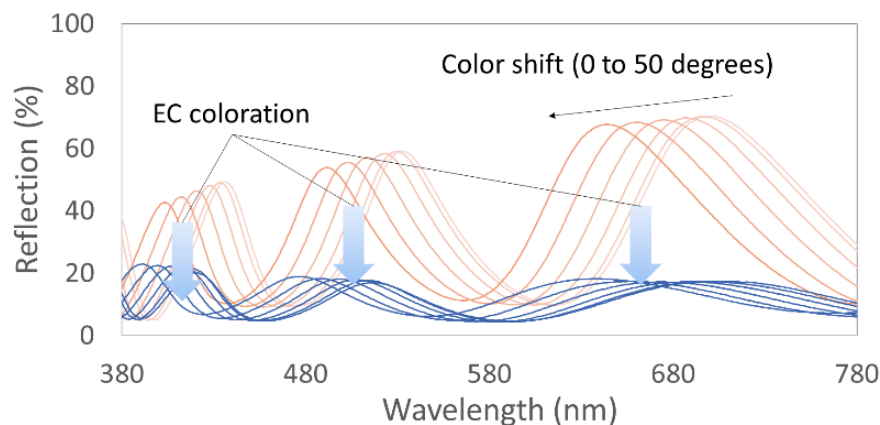Figure 5.4: ATF color-shifting electrochromic device

Figure 5.5: Reflection spectra in the bleached (orange) and colored states (blue).

Although the color was satisfactory, the dynamics still left much to be improved. Most notably, voltages of +7 and -8 V were required for the operation and the coloration time took upwards of 30 seconds (see Figure 5.6). Ideally, this type of security device should be operable with 1-2 V and
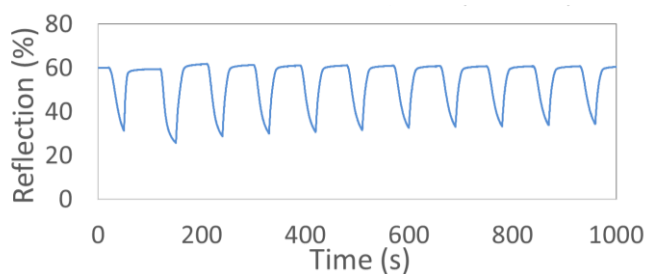

Figure 5.6: *In situ* coloration and bleaching cycles at +7 V and -8 V at 533 nm.

have a visible color change within a few seconds.

To improve these parameters, the solution was to modify the electrolyte deposition process. The presence of self-bleaching and the need for an excessive potential for switching in the previous devices indicated that the electrolyte layer was not acting as a proper electron barrier. One way to fix this problem is to increase its thickness, but the devices we prepared with very thick electrolytes had reduced speed of coloration. Another method, proposed in the literature suggests that the deposition conditions of the Ta_2O_5 are critical to its electrical properties and that a SiO_2 interlayer can have a drastic effect on the overall electrical behavior [56]. Thus, deposition of the Ta_2O_5 layer

in two steps to mitigate the propagation of growth defects and the addition of a thin silica layer (15 nm) led to much more promising devices (see Figure 5.7).
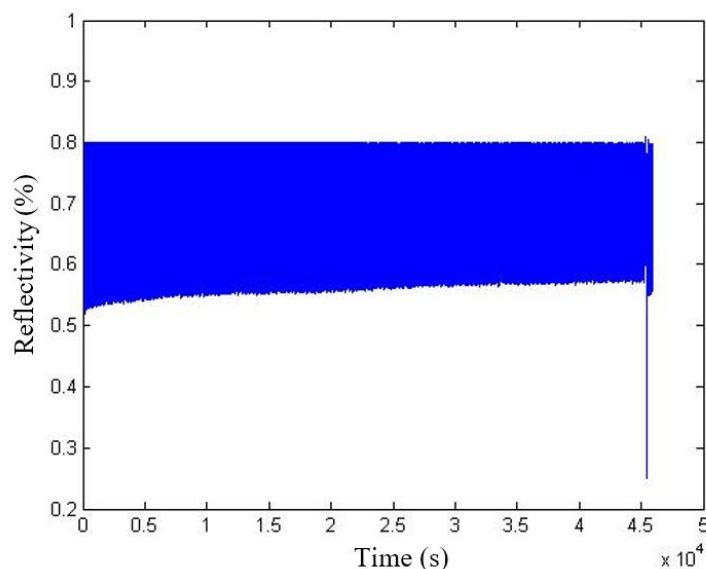

Figure 5.7: Coloration test over 900 cycles of an ATF electrochromic device with a Fabry-Perot-like metal-dielectric architecture. The applied potential was ±3 V and coloration/bleaching times are 10 s. A more intense cycle at the end resulted in the partial rejuvenation of the device.

The device now exhibits a sufficient amount of coloration at a reasonable applied potential, but the coloration time is still slightly too long at 10 s. Observing that the edges of the surface were switching much faster, we decided to pattern the top electrode in the shape of a Moore curve known to maximize the perimeter over the area ratio. The resulting device did achieve a faster coloration with visible change after 2-3 s, indicating that surface patterning and image design can be an important factor in conceiving a high-performance device (see Figure 5.8).

Although some work remains to be made, particularly on the deposited electrodes' quality, the device creation process is now sufficiently mastered to try and replace the WO_3 layer with the biased version developed during this project. This is a promising next step in this project that could result in further performance improvements and demonstrate the use of such layers in a concrete application.
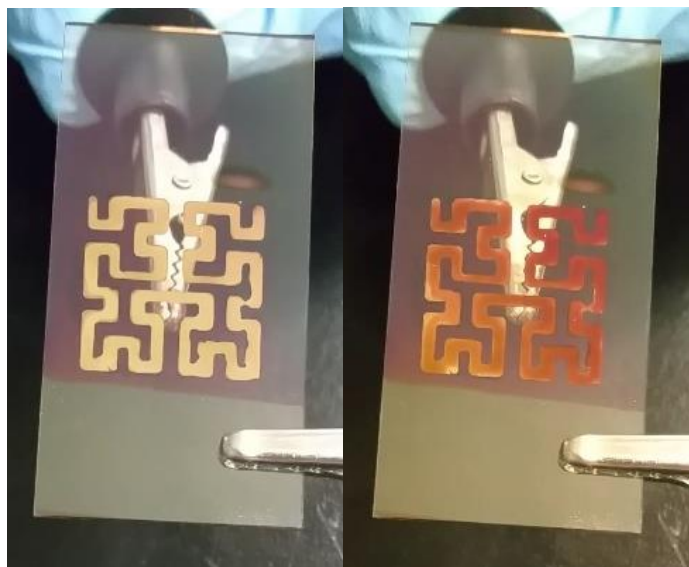
Figure 5.8: Coloration test of Moore-curve-patterned device. Bleached (left) and colored for 3 s at -3 V (right).

CHAPTER 6   CONCLUSION AND RECOMMENDATIONS

According to the results obtained during this project, substrate biasing and high energy ion bombardment is a promising way of improving the electrochemical properties of WO_3 thin films. It results in structural changes that give a significant increase in durability while maintaining performance similar to that of regular layers deposited at 20 mTorr. The ability to sputter at lower pressures —1 mTorr in the present case — also results in a five-fold increase in deposition rate in our system, a major advantage in the context of production on an industrial scale.

In parallel with the work on WO_3, significant advances were made in the fabrication of all-thin-film electrochromic devices in the context of security devices. An innovative approach involving two-levels of authentication in a device incorporating both an active color change and an angular color shift was demonstrated, along with improvements upon the initial design to achieve greater coloration speed at lower applied potentials.

Based on these findings, improving our control over the substrate biasing process could lead to additional refining of the ideal microstructure for ion insertion in WO_3. A more in-depth study of the effect of heating and the respective role of each of the two identified phases promises to give important insights on the process and could be the basis for further study, which should include modeling and simulation of the layer growth depending on the energy and flux of the ion bombardment. Using ion beams to generate the ion bombardment in a more controlled manner would be an interesting alternative. Combining the biased WO_3 layer and the security devices for improved performance is also envisioned to have potential as a future research project Another pathway is to add color effects in smart EC windows, giving more variety to architectural designs.

BIBLIOGRAPHY

[1]   British Petroleum, "BP Statistical Review of World Energy 2017," *Br. Pet.*, no. 66, pp. 1–52, 2017.

[2]   O. Ellabban, H. Abu-Rub, and F. Blaabjerg, "Renewable energy resources: Current status, future prospects and their enabling technology," *Renew. Sustain. Energy Rev.*, vol. 39, pp. 748–764, 2014.

[3]   United Nations Environment Programme, *Buildings and Climate Change: Status, Challenges and Opportunities*. 2007.

[4]   J. A. Leech, W. C. Nelson, R. T. Burnett, S. Aaron, and M. E. Raizenne, "It's about time: A comparison of Canadian and American time-activity patterns," *J. Expo. Anal. Environ. Epidemiol.*, vol. 12, no. 6, pp. 427–432, 2002.

[5]   M. B. C. Aries, J. A. Veitch, and G. R. Newsham, "Windows, view, and office characteristics predict physical and psychological discomfort," *J. Environ. Psychol.*, vol. 30, no. 4, pp. 533–541, 2010.

[6]   C. G. Granqvist, A. Azens, A. Hjelm, L. Kullman, G. A. Niklasson, D. Rönnow, M. Strømme Mattsson, M. Veszelei, and G. Vaivars, "Recent advances in electrochromics for smart windows applications," *Sol. Energy*, vol. 63, no. 4, pp. 199–216, 1998.

[7]   B. P. Jelle, "Solar radiation glazing factors for window panes, glass structures and electrochromic windows in buildings - Measurement and calculation," *Sol. Energy Mater. Sol. Cells*, vol. 116, no. 7465, pp. 291–323, 2013.

[8]   S. C. Drumheller, C. Köhler, and S. Minen, "Field evaluation of low-e storm windows," in *Thermal Performance of Exterior Envelopes of Whole Buildings X International Conference*, 2007.

[9]   R. T. Wen, M. A. Arvizu, G. A. Niklasson, and C. G. Granqvist, "Electrochromics for energy efficient buildings: Towards long-term durability and materials rejuvenation," *Surf. Coatings Technol.*, vol. 290, pp. 135–139, 2016.

[10]   L. M. Huang, C. W. Hu, H. C. Liu, C. Y. Hsu, C. H. Chen, and K. C. Ho, "Photovoltaic

electrochromic device for solar cell module and self-powered smart glass applications," *Sol. Energy Mater. Sol. Cells*, vol. 99, no. November, pp. 154–159, 2012.

[11] H. Camirand, B. Baloukas, J. E. Klemberg-Sapieha, and L. Martinu, "In situ spectroscopic ellipsometry of electrochromic amorphous tungsten oxide films," *Sol. Energy Mater. Sol. Cells*, vol. 140, pp. 77–85, 2015.

[12] B. Baloukas, J. M. Lamarre, and L. Martinu, "Electrochromic interference filters fabricated from dense and porous tungsten oxide films," *Sol. Energy Mater. Sol. Cells*, vol. 95, no. 3, pp. 807–815, 2011.

[13] N. Martin, D. Baretti, C. Rousselot, and J.-Y. Rauch, "The effect of bias power on some properties of titanium and titanium oxide films prepared by r.f. magnetron sputtering," *Surf. Coatings Technol.*, vol. 107, pp. 172–182, 1998.

[14] L. Y. Liang, H. T. Cao, Q. Liu, K. M. Jiang, Z. M. Liu, F. Zhuge, and F. L. Deng, "Substrate biasing effect on the physical properties of reactive RF-magnetron-sputtered aluminum oxide dielectric films on ITO glasses," *ACS Appl. Mater. Interfaces*, vol. 6, no. 4, pp. 2255–2261, 2014.

[15] B. Baloukas, "Thin Film-Based Optically Variable Security Devices : From Passive to Active," 2012.

[16] C. G. Granqvist, *Handbook of Inorganic Electrochromic Materials*, First ed. Amsterdam, 1995.

[17] P. M. S. Monk, R. J. Mortimer, and D. R. Rosseinsky, *Electrochromism and electrochromic devices*, Second ed. Cambridge, 2007.

[18] P. R. Somani and S. Radhakrishnan, "Electrochromic Materials and Devices," *Mater. Chem. Phys.*, vol. 77, p. 117, 2002.

[19] R. J. Mortimer, " Electrochromic Materials," *Annu. Rev. Mater. Res*, vol. 41, pp. 241–68, 2011.

[20] G. A. Niklasson, L. Berggren, and A. L. Larsson, "Electrochromic tungsten oxide: The role of defects," in *Solar Energy Materials and Solar Cells*, 2004, vol. 84, no. 1–4, pp. 315–328.

[21] H. N. Hersh, W. E. Kramer, and J. H. McGee, "Mechanism of electrochromism in WO_3,"

Appl. Phys. Lett., vol. 27, no. 12, pp. 646–648, 1975.

[22] K. Bange, "Colouration of tungsten oxide films: A model for optically active coatings," *Sol. Energy Mater. Sol. Cells*, vol. 58, no. 1, pp. 1–131, 1999.

[23] C. Li, J. H. Hsieh, M. T. Hung, and B. Q. Huang, "Electrochromic study on amorphous tungsten oxide films by sputtering," *Thin Solid Films*, vol. 587, pp. 75–82, 2015.

[24] C. G. Granqvist, "Electrochromic tungsten oxide films: Review of progress 1993-1998," *Sol. Energy Mater. Sol. Cells*, vol. 60, no. 3, pp. 201–262, 2000.

[25] S. Darmawi, S. Burkhardt, T. Leichtweiss, D. A. Weber, S. Wenzel, and J. Janek, "Correlation of electrochromic properties and oxidation states in nanocrystalline tungsten trioxide †," *Phys. Chem. Chem. Phys.*, vol. 17, no. 2, pp. 15903–15911, 2015.

[26] C. G. Granqvist, "Electrochromics for smart windows: Oxide-based thin films and devices," *Thin Solid Films*, vol. 564. pp. 1–38, 2014.

[27] A. C. Dillon, A. H. Mahan, R. Deshpande, P. A. Parilla, K. M. Jones, and S. H. Lee, "Metal oxide nano-particles for improved electrochromic and lithium-ion battery technologies," *Thin Solid Films*, vol. 516, no. 5, pp. 794–797, 2008.

[28] M. A. Arvizu, C. A. Triana, B. I. Stefanov, C. G. Granqvist, and G. A. Niklasson, "Electrochromism in sputter-deposited W-Ti oxide films: Durability enhancement due to Ti," *Sol. Energy Mater. Sol. Cells*, vol. 125, pp. 184–189, 2014.

[29] R. J. D. Tilley, "The crystal chemistry of the higher tungsten oxides," *Int. J. Refract. Met. Hard Mater.*, vol. 13, no. 1–3, pp. 93–109, 1995.

[30] T. C. Arnoldussen, "A Model for Electrochromic Tungstic Oxide Microstructure and Degradation," *J. Electrochem. Soc.*, vol. 128, no. 1, pp. 117–123, 1981.

[31] T. Nanba and I. Yasui, "X-ray diffraction study of microstructure of amorphous tungsten trioxide films prepared by electron beam vacuum evaporation," *J. Solid State Chem.*, vol. 315, pp. 304–315, 1989.

[32] S. Sallard, T. Brezesinski, and B. M. Smarsly, "Electrochromic stability of WO_3 thin films with nanometer-scale periodicity and varying degrees of crystallinity," *J. Phys. Chem. C*, vol. 111, no. 19, pp. 7200–7206, 2007.

[33] M. Deepa, a K. Srivastava, M. Kar, and S. a Agnihotry, "A case study of optical properties and structure of sol–gel derived nanocrystalline electrochromic WO_3 films," *J. Phys. D. Appl. Phys.*, vol. 39, no. 9, pp. 1885–1893, 2006.

[34] M. Ohring, *The Materials Science of Thin Films*. Academic Press, 1992.

[35] M. B. Johansson, B. Zietz, G. a. Niklasson, and L. Österlund, "Optical properties of nanocrystalline WO_3 and $WO_{(3-x)}$ thin films prepared by DC magnetron sputtering," *J. Appl. Phys.*, vol. 115, no. 21, p. 213510, 2014.

[36] M. H. Kim, H. W. Choi, and K. H. Kim, "Properties of WO_{3-x} Electrochromic Thin Film Prepared by Reactive Sputtering with Various Post Annealing Temperatures," *Jpn. J. Appl. Phys.*, vol. 52, no. 11S, p. 11NB09, 2013.

[37] A. Anders, "A structure zone diagram including plasma-based deposition and ion etching," *Thin Solid Films*, vol. 518, no. 15, pp. 4087–4090, 2010.

[38] Cuomo, J.J., Rossnagel, S.M., and Kaufman, H.R., *Handbook of ion beam processing technology*. United States, Park Ridge, NJ, Noyes, 1989.

[39] A. S. Reddy, G. Venkata Rao, S. Uthanna, and P. Sreedhara Reddy, "Influence of substrate bias voltage on the properties of magnetron sputtered Cu_2O films," *Phys. B Condens. Matter*, vol. 370, no. 1–4, pp. 29–34, 2005.

[40] V. Madhavi, P. Kondaiah, and S. Uthanna, "Influence of substrate bias voltage on structural and optical properties of RF reactive magnetron sputtered WO3 thin films," *J. Phys. Conf. Ser.*, vol. 390, p. 12059, 2012.

[41] K. Cang, L. Y. Liang, Z. M. Liu, L. Wu, H. Luo, H. T. Cao, and Y. S. Zou, "Influence of the substrate bias voltage on the physical properties of dc reactive sputtered Ta_2O_5 films," *J. Alloys Compd.*, vol. 550, pp. 258–262, 2013.

[42] A. P. Giri and R. Messier, "Physical structure and the electrochromic effect in WO_3," in *MRS Proceedings, Vol.24*, 1983, pp. 221–227.

[43] J. A. Woollam Co., *CompleteEASE^{TM} Data Analysis Manual*. 2009.

[44] Y. Shigesato, A. Murayama, T. Kamimori, and K. Matsuhiro, "Characterization of evaporated amorphous WO3films by Raman and FTIR spectroscopies," *Appl. Surf. Sci.*, vol.

33–34, no. C, pp. 804–811, 1988.

[45]   C. G. Granqvist, "Oxide electrochromics: An introduction to devices and materials," *Sol. Energy Mater. Sol. Cells*, vol. 99, pp. 1–13, 2012.

[46]   S. H. Lee, R. Deshpande, P. A. Parilla, K. M. Jones, B. To, A. H. Mahan, and A. C. Dillon, "Crystalline WO_3 nanoparticles for highly improved electrochromic applications," *Adv. Mater.*, vol. 18, no. 6, pp. 763–766, 2006.

[47]   S. Hashimoto and et. Al., "Electrochromic device and method for manufacturing the same. U.S. Patent no. 5777779." United States Patent, Tokyo, p. U.S. Patent nos. 5777779, 1–13, 1998.

[48]   D. Brassard, M. A. El Khakani, and L. Ouellet, "Substrate biasing effect on the electrical properties of magnetron-sputtered high-k titanium silicate thin films," *J. Appl. Phys.*, vol. 102, no. 3, p. 34106, 2007.

[49]   Y. Shigesato, A. Murayama, T. Kamimori, and K. Matsuhiro, "Characterization of evaporated amorphous WO_3 films by Raman and FTIR spectroscopies," *Appl. Surf. Sci.*, vol. 33–34, no. C, pp. 804–811, 1988.

[50]   D. Li, M. Carette, A. Granier, J. P. Landesman, and A. Goullet, "Effect of ion bombardment on the structural and optical properties of TiO_2 thin films deposited from oxygen/titanium tetraisopropoxide inductively coupled plasma," *Thin Solid Films*, vol. 589, pp. 783–791, 2015.

[51]   K. Oughstun and N. Cartwright, "On the Lorentz-Lorenz formula and the Lorentz model of dielectric dispersion: addendum," *Opt. Express*, vol. 11, no. 13, pp. 1541–1546, 2003.

[52]   A. Azens, C. G. Granqvist, E. Pentjuss, J. Gabrusenoks, and J. Barczynska, "Electrochromism of fluorinated and electron-bombarded tungsten oxide films," *J. Appl. Phys.*, vol. 78, no. 3, pp. 1968–1974, 1995.

[53]   T.-S. Yang, Z.-R. Lin, and M.-S. Wong, "Structures and electrochromic properties of tungsten oxide films prepared by magnetron sputtering," *Appl. Surf. Sci.*, vol. 252, no. 5, pp. 2029–2037, 2005.

[54]   M. Deepa, A. K. Srivastava, S. Singh, and S. a. Agnihotry, "Structure–property correlation

of nanostructured WO_3 thin films produced by electrodeposition," *J. Mater. Res.*, vol. 19, no. January, p. 2576, 2004.

[55] R. W. Phillips and a F. Bleikolm, "Optical coatings for document security.," *Appl. Opt.*, vol. 35, no. 28, pp. 5529–5534, 1996.

[56] S. B. Shen, I. Chen, J. Bohlman, G. Brown, R. Doering, and T. Austin, "Conduction mechanisms in sputtered Ta_2O_5 on Si with an interfacial SiO_2 layer", *J. Appl. Phys.* vol. 65, no. 3, pp.1140-1146, 1989.

[57] Electrochromic Laminated Glass product information, Gesimat, 2009, retrieved January 2018, www.gesimat.de
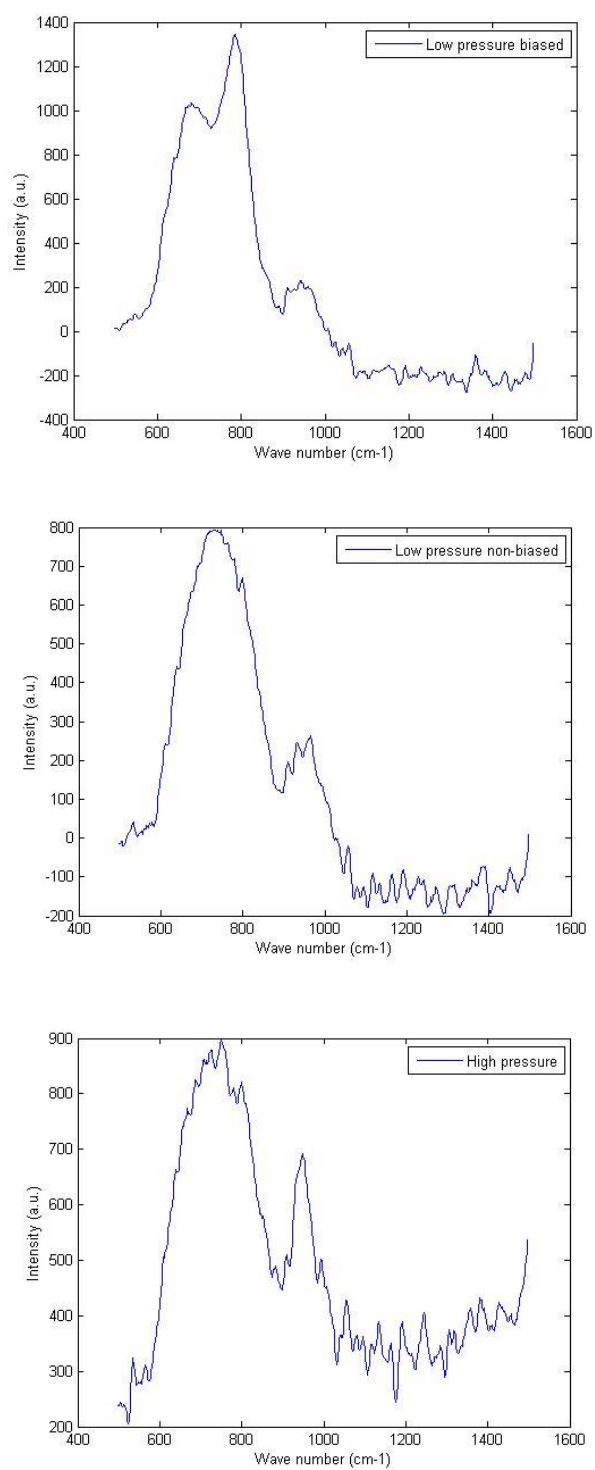
APPENDIX A – ARTICLE SUPPLEMENTARY DATA

Figure S1: Raman spectra for the biased, non-biased and high-pressure samples